

26 **§Corresponding author:** Lúcia Helena Faccioli, Ph.D. (faccioli@fcfrp.usp.br)
27 Departamento de Análises Clínicas, Toxicológicas e Bromatológicas. Faculdade de
28 Ciências Farmacêuticas de Ribeirão Preto - FCFRP, Universidade de São Paulo - USP
29 Av. do Café, s/n - Vila Monte Alegre, Ribeirão Preto - SP, 14040-900, Ribeirão Preto,
30 São Paulo, Brazil. FCFRP-USP, Bloco S, Sala 96A.
31
32 1 - Departamento de Análises Clínicas, Toxicológicas e Bromatológicas. Faculdade de
33 Ciências Farmacêuticas de Ribeirão Preto - FCFRP, Universidade de São Paulo - USP,
34 Ribeirão Preto, São Paulo, Brazil;
35 2 - Departamento de Bioquímica e Imunologia. Faculdade de Medicina de Ribeirão Preto
36 - FMRP, Universidade de São Paulo-USP, São Paulo, Brazil;
37 3 - Departamento de Cirurgia e Anatomia, Faculdade de Medicina de Ribeirão Preto -
38 FMRP, Universidade de São Paulo-USP, Ribeirão Preto, São Paulo, Brazil;
39 4 - Departamento de Clínica Médica, Faculdade de Medicina de Ribeirão Preto - FMRP,
40 Universidade de São Paulo-USP, São Paulo, Brazil;
41 5 - Departamento de Química. Faculdade de Filosofia, Ciências e Letras de Ribeirão Preto
42 - FFCLRP. Universidade de São Paulo-USP, Ribeirão Preto, São Paulo, Brazil;
43 6 - Departamento de Genética e Evolução, Centro de Ciências Biológicas e da Saúde
44 Universidade Federal de São Carlos - UFSCar, São Carlos, São Paulo, Brazil;
45 7 - Programa de Pós-graduação em Imunologia Básica e Aplicada, Faculdade de Medicina
46 de Ribeirão Preto - FMRP, Universidade de São Paulo-USP, Ribeirão Preto São Paulo,
47 Brazil;

- 48 8 - Programa de Pós-graduação em Biociências e Biotecnologia Aplicadas à Farmácia,
49 Faculdade de Ciências Farmacêuticas de Ribeirão Preto - FCFRP, Universidade de São
50 Paulo - USP, Ribeirão Preto, São Paulo, Brazil;
- 51 9 - Programa de Pós-graduação em Imunologia Básica e Aplicada, Instituto de Ciências
52 Biológicas, Universidade Federal do Amazonas - UFAM, Manaus, Amazonas, Brazil;
- 53 10 - Departamento de Enfermagem Materno-Infantil e Saúde Pública, Escola de
54 Enfermagem de Ribeirão Preto - EERP, Universidade de São Paulo-USP, Ribeirão Preto,
55 São Paulo, Brazil;
- 56 11 - Departamento de Enfermagem Geral e Especializada, Escola de Enfermagem de
57 Ribeirão Preto - EERP, Universidade de São Paulo-USP, Ribeirão Preto, São Paulo,
58 Brazil;
- 59 12 - Instituto de Patologia Tropical e Saúde Pública, Universidade Federal de Goiás -
60 UFG, Goiânia, Goiás, Brazil;
- 61 13 - Hospital Santa Casa de Misericórdia de Ribeirão Preto, Ribeirão Preto, São Paulo,
62 Brazil;
- 63 14 - Hospital São Paulo, Ribeirão Preto, São Paulo, Brazil.

64 **Abstract**

65 Cytokine storms and hyperinflammation, potentially controlled by glucocorticoids, occur
66 in COVID-19; the roles of lipid mediators and acetylcholine (ACh) and how
67 glucocorticoid therapy affects their release in Covid-19 remain unclear. Blood and
68 bronchoalveolar lavage (BAL) samples from SARS-CoV-2- and non-SARS-CoV-2-
69 infected subjects were collected for metabolomic/lipidomic, cytokines, soluble CD14
70 (sCD14), and ACh, and CD14 and CD36-expressing monocyte/macrophage
71 subpopulation analyses. Transcriptome reanalysis of pulmonary biopsies was performed
72 by assessing coexpression, differential expression, and biological networks. Correlations
73 of lipid mediators, sCD14, and ACh with glucocorticoid treatment were evaluated. This
74 study enrolled 190 participants with Covid-19 at different disease stages, 13 hospitalized
75 non-Covid-19 patients, and 39 healthy-participants. SARS-CoV-2 infection increased
76 blood levels of arachidonic acid (AA), 5-HETE, 11-HETE, sCD14, and ACh but
77 decreased monocyte CD14 and CD36 expression. 5-HETE, 11-HETE, cytokines, ACh,
78 and neutrophils were higher in BAL than in circulation (fold-change for 5-HETE 389.0;
79 11-HETE 13.6; ACh 18.7, neutrophil 177.5, respectively). Only AA was higher in
80 circulation than in BAL samples (fold-change 7.7). Results were considered significant
81 at $P < 0.05$, 95%CI. Transcriptome data revealed a unique gene expression profile
82 associated with AA, 5-HETE, 11-HETE, ACh, and their receptors in Covid-19.
83 Glucocorticoid treatment in severe/critical cases lowered ACh without impacting disease
84 outcome. We first report that pulmonary inflammation and the worst outcomes in Covid-
85 19 are associated with high levels of ACh and lipid mediators. Glucocorticoid therapy
86 only reduced ACh, and we suggest that treatment may be started early, in combination
87 with AA metabolism inhibitors, to better benefit severe/critical patients.

88 **Introduction**

89 Individuals Covid-19 may present asymptotically or with manifestations
90 ranging from acute respiratory distress syndrome to systemic hyperinflammation and
91 organ failure, events attributed to cytokine storms¹. Free polyunsaturated fatty acids, such
92 as AA and derivative eicosanoids, regulate inflammation^{2,3}, yet their role in Covid-19 has
93 not been well investigated.

94 ACh, which is released by nerves⁴, leukocytes⁵, and airway epithelial cells⁶,
95 regulates metabolism⁷, cardiac function⁸, airway inflammation⁹, and cytokine
96 production¹⁰, all of which occur in Covid-19. It is known that eicosanoids stimulate ACh
97 release³, but crosstalk between cholinergic and lipid mediator pathways in Covid-19 still
98 need to be clarified.

99 In this study, levels of lipid mediators, ACh, and other inflammatory markers in
100 blood and BAL from patients with Covid-19 who were treated or not with glucocorticoids
101 were compared to those of non-Covid-19 and healthy-participants. Moreover, lung biopsy
102 transcriptome reanalysis data from Covid-19 and non-Covid-19 patients corroborated our
103 findings.

104 **Methods**

105 **Study design and blood collection**

106 This observational, analytic, and transversal study was conducted from June to
107 November 2020. All participants were over 16 years old and chosen according to the
108 inclusion and exclusion criteria described in Table S1 and in the protocol, after providing
109 signed consent. Blood samples collected from patients positive for Covid-19 (n=190)
110 were analyzed by RT-qPCR (Biomol OneStep/Covid-19 kit; Institute of Molecular
111 Biology of Paraná - IBMP Curitiba/PR, Brazil) using nasopharyngeal swabs and/or

112 serological assays to detect IgM/IgG/IgA (SARS-CoV-2[®] antibody test; Guangzhou
113 Wondfo Biotech, China). Samples obtained from a cohort of SARS-CoV-2-negative
114 healthy participants were used as controls (n=39). Participants positive for Covid-19 were
115 categorised as asymptomatic-mild (n=43), moderate (n=44), severe (n=54), or critical
116 (n=49). The criteria for the clinical classification of patients were defined at the time of
117 sample collection, as shown in Table S1. Peripheral blood samples were obtained by
118 venous puncture from patients upon their first admission and/or during the period of
119 hospitalisation at two medical centres, *Santa Casa de Misericórdia de Ribeirão Preto* and
120 *Hospital Sao Paulo* at Ribeirão Preto, São Paulo State, Brazil. Blood samples from
121 healthy controls and asymptomatic-mild non-hospitalized participants were collected
122 either at the Centre of Scientific and Technological Development “Supera Park”
123 (Ribeirão Preto, São Paulo State, Brazil) or in the home of patients receiving at-home
124 care. The plasma was separated from whole blood samples and stored at -80°C. For
125 lipidomic and metabolomic analyses, 250 µL of plasma was stored immediately in
126 methanol (1:1 v/v). Lipidomic and metabolomic analyses were performed by mass
127 spectrometry (LC-MS/MS), while a cytokines, sCD14, and ACh were quantified using
128 CBA flex Kit (flow cytometer assay) or commercial ELISA. The expression levels of
129 CD14, CD36, CD16, and HLA-DR in cells were evaluated by flow cytometry following
130 the gate strategy (Figure S2).

131 **Ethical considerations**

132 All participants provided written consent in accordance with the regulations of the
133 *Conselho Nacional de Pesquisa em Humanos* (CONEP) and the Human Ethical
134 Committee from *Faculdade de Ciências Farmacêuticas de Ribeirão Preto* (CEP-FCFRP-
135 USP). The research protocol was approved and received the certificate of Presentation
136 and Ethical Appreciation (CAAE: 30525920.7.0000.5403). The sample size was

137 determined by the convenience of sampling, availability at partner hospitals, agreement
138 to participate, and the pandemic conditions within the local community (more information
139 in the Protocol).

140 **Bronchoalveolar lavage fluid (BAL) collection and processing**

141 BAL fluids were collected from hospitalised Covid-19 patients at the severe or critical
142 stages of disease (n=32) to assess their lung immune responses. Control samples were
143 obtained from hospitalised intubated donors negative for SARS-CoV-2 (n=13) (as
144 certified by SARS-CoV-2-negative PCR), referred to as non-Covid-19 patients, who were
145 intubated because of the following primary conditions: bacterial pneumonia, abdominal
146 septic shock associated with respiratory distress syndrome, pulmonary atelectasis due to
147 phrenic nerve damage, or pulmonary tuberculosis. BAL fluid was collected as previously
148 described¹¹, using a siliconized polyvinylchloride catheter (Mark Med, Porto Alegre,
149 Brazil) with a closed Trach Care endotracheal suction system (Bioteque Corporation,
150 Chirurgic Fernandes Ltd., Santana Parnaíba, Brazil) and sterile 120 mL polypropylene
151 flask (Biomeg-Biotec Hospital Products Ltd., Mairiporã, Brazil) under aseptic conditions.
152 Approximately 5–10 mL of bronchoalveolar fluid was obtained and placed on ice for
153 processing within 4 h. The BAL fluids were placed into 15-mL polypropylene collection
154 tubes and received half volume of their volume of phosphate buffered saline (PBS) 0.1
155 M (2:1 v/v) in relation to the total volume of each sample. After centrifugation (700 × g,
156 10 min), the supernatants of the BAL fluid were recovered and stored at –80°C. For
157 lipidomic and metabolomic analyses, 250 µL of these supernatants were stored
158 immediately in methanol (1:1 v/v). Subsequently, the remaining BAL fluid was diluted in
159 10 mL of PBS and gently filtered through a 100-µm cell strainer (Costar, Corning, NY,
160 USA) using a syringe plunger. The resulting material was used for cytokine and
161 acetylcholine (ACh) quantification. The BAL fluids were centrifuged (700 × g, 10 min)

162 and the red blood cells were lysed using 1 mL of ammonium chloride (NH₄Cl) buffer
163 0.16 M for 5 min. The remaining airway cells were washed with 10 mL of PBS,
164 resuspended in PBS–2% heat-inactivated foetal calf serum, and counted with Trypan blue
165 using an automated cell counter (Countess, Thermo Fisher Scientific, Waltham, MA,
166 USA). The leukocyte numbers were adjusted to 1×10^9 cells/L for differential counts and
167 1×10^6 cells/mL for flow cytometry analysis. All procedures were performed in a Level
168 3 Biosafety Facility (*Departamento de Bioquímica e Imunologia, Faculdade de Medicina*
169 *de Ribeirão Preto, Universidade de São Paulo*).

170 **Data collection**

171 The electronic medical records of each patient were carefully reviewed. Data
172 included sociodemographic information, comorbidities, medical history, clinical
173 symptoms, routine laboratory tests, immunological tests, chest computed tomography
174 (CT) scans, clinical interventions, and outcomes (more information in the Protocol). The
175 information was documented on a standardised record form, as indicated in Tables S1,
176 S2, and S3. Data collection of laboratory results included first-time examinations within
177 24 h of admission, defined as the primary endpoint. The secondary endpoint was clinical
178 outcome (death or recovery).

179 **Clinical laboratory collection**

180 For hospitalised patients, blood examinations were performed by clinical analysis
181 laboratories at their respective hospitals. Blood examinations of healthy participants and
182 non-hospitalized patients were performed at *Serviço de Análises Clínicas (SAC),*
183 *Departamento de Análises Clínicas, Toxicológicas e Bromatológicas* of the *Faculdade*
184 *de Ciências Farmacêuticas de Ribeirão Preto, Universidade de São Paulo, Ribeirão*

185 *Preto, São Paulo, Brazil*. The blood samples were used to measure for liver and kidney
186 function, myocardial enzyme spectrum, coagulation factors, red blood cells,
187 haemoglobin, platelets, and total and differential leukocytes using automated equipment.
188 Similarly, the absolute numbers of leukocytes in the BAL fluid were determined in a
189 Neubauer Chamber with Turkey solution. For the counts of differential leukocytes in the
190 BAL, 100 μ L of the fluid was added to cytopsin immediately after collection to avoid any
191 interference on cell morphology. Differential leukocyte counts were conducted using an
192 average of 200 cells after staining with Fast Panoptic (LABORCLIN; Laboratory
193 Products Ltd, Pinhais, Brazil) and examined under an optical microscope (Zeiss EM109;
194 Carl Zeiss AG, Oberkochen, Germany) with a 100 \times objective (immersion oil) equipped
195 with a Veleta CCD digital camera (Olympus Soft Imaging Solutions GmbH, Germany)
196 and ImageJ (1.45s) (National Institutes of Health, Rockville, MD, USA)¹². Lymphocytes,
197 neutrophils, eosinophils, and monocytes/macrophages were identified and
198 morphologically characterised, and their lengths and widths were measured (100 \times).

199 **High-performance liquid chromatography coupled with tandem Mass Spectrometry**
200 **(LC-MS/MS) assay**

201 ***Reagents***

202 Eicosanoids, free fatty acids (AA, EPA, and DHA), and metabolites as molecular
203 weight standards (MWS) and deuterated internal standards were purchased from Cayman
204 Chemical Co. (Ann Arbor, MI, USA). HPLC-grade acetonitrile (ACN), methanol
205 (MeOH), and isopropanol were purchased from Merck (Kenilworth, NJ, USA). Ultrapure
206 deionised water (H₂O) was obtained using a Milli-Q water purification system (Merck-
207 Millipore, Kenilworth, NJ, USA). Acetic acid (CH₃COOH) and ammonium hydroxide
208 (NH₄OH) were obtained from Sigma Aldrich (St. Louis, MO, USA).

209 *Sample preparation and extraction*

210 The plasma (250 μ L) in EDTA-containing tubes (Vacutainer[®] EDTA K2; BD
211 Diagnostics, Franklin Lakes, NJ, USA) and BAL (250 μ L) samples were stored in MeOH
212 (1:1, v/v) at -80°C . Three additional volumes of ice-cold absolute MeOH were added to
213 each sample overnight at -20°C for protein denaturation and after lipid solid-phase
214 extraction (SPE). To each sample, 10 μ L of internal standard (IS) solution was added,
215 centrifuged at $800 \times g$ for 10 min at 4°C . The resulting supernatants were collected and
216 diluted with deionised water (ultrapure water; Merck-Millipore, Kenilworth, NJ, USA) to
217 obtain a MeOH concentration of 10% (v/v). In the SPE extractions, a Hypersep C18-500
218 mg column (3 mL) (Thermo Scientific-Bellefonte, PA, USA) equipped with an extraction
219 manifold collector (Waters-Milford, MA, USA) was used. The diluted samples were
220 loaded into the pre-equilibrated column and washing using 2 mL of MeOH and H₂O
221 containing 0.1% acetic acid, respectively. Then, the cartridges were flushed with 4 mL of
222 H₂O containing 0.1% acetic acid to remove hydrophilic impurities. The lipids that had
223 been adsorbed on the SPE sorbent were eluted with 1 mL of MeOH containing 0.1%
224 acetic acid. The eluates solvent was removed in vacuum (Concentrator Plus, Eppendorf,
225 Germany) at room temperature and reconstituted in 50 μ L of MeOH/H₂O (7:3, v/v) for
226 LC-MS/MS analysis.

227 *LC-MS/MS analysis and lipids data processing*

228 Liquid chromatography was performed using an Ascentis Express C18 column
229 (Supelco, St. Louis, MO, USA) with 100×4.6 mm and a particle size of 2.7 μm in a high-
230 performance liquid chromatography (HPLC) system (Nexera X2; Shimadzu, Kyoto,
231 Japan). Then, 20 μ L of extracted sample was injected into the HPLC column. Elution was
232 carried out under a binary gradient system consisting of Phase A, comprised of H₂O,

233 ACN, and acetic acid (69.98:30:0.02, v/v/v) at pH 5.8 (adjusted with NH₄OH), and Phase
234 B, comprised of ACN and isopropanol (70:30, v/v). Gradient elution was performed for
235 25 min at a flow rate of 0.5 mL/min. The gradient conditions were as follows: 0 to 2 min,
236 0% B; 2 to 5 min, 15% B; 5 to 8 min, 20% B; 8 to 11 min, 35% B; 11 to 15 min, 70% B;
237 and 15 to 19 min, 100% B. At 19 min, the gradient was returned to the initial condition
238 of 0% B, and the column was re-equilibrated until 25 min. During analysis, the column
239 samples were maintained at 25°C and 4°C in the auto-sampler. The HPLC system was
240 directly connected to a TripleTOF 5600+ mass spectrometer (SCIEX-Foster, CA, USA).
241 An electrospray ionisation source (ESI) in negative ion mode was used for high-resolution
242 multiple-reaction monitoring (MRM^{HR}) scanning. An atmospheric-pressure chemical
243 ionisation probe (APCI) was used for external calibrations of the calibrated delivery
244 system (CDS). Automatic mass calibration (<2 ppm) was performed periodically after
245 each of the five sample injections using APCI Negative Calibration Solution (Sciex-
246 Foster, CA, USA) injected via direct infusion at a flow rate of 300 µL/min. Additional
247 instrumental parameters were as follows: nebuliser gas (GS1), 50 psi; turbo gas (GS2),
248 50 psi; curtain gas (CUR), 25 psi; electrospray voltage (ISVF), -4.0 kV; temperature of
249 the turbo ion spray source, 550°C. The dwell time was 10 ms, and a mass resolution of
250 35,000 was achieved at *m/z* 400. Data acquisition was performed using AnalystTM
251 software (SCIEX- Foster, CA, USA). Qualitative identification of the lipid species was
252 performed using PeakViewTM (SCIEX-Foster, CA, USA). MultiQuantTM (SCIEX-Foster,
253 CA, USA) was used for the quantitative analysis, which allows the normalisation of the
254 peak intensities of individual molecular ions using an internal standard for each class of
255 lipid. The quantification of each compound was performed using internal standards and
256 calibration curves, and the specific mass transitions of each lipid were determined

257 according to our previously published method¹³. The final concentration of lipids was
258 normalised by the initial volume of plasma or BAL fluid (ng/mL).

259 ***Metabolomics analysis***

260 Metabolite was extracted and samples were transferred to autosampler vials for
261 LC–MS analysis using TripleTOF5600+ Mass Spectrometer (Sciex-Foster, CA, USA)
262 coupled to an ultra-high-performance liquid chromatography (UHPLC) system (Nexera
263 X2; Shimadzu, Kyoto, Japan). Reverse-phase chromatography was performed similarly
264 to lipids analyses above. Mass spectral data were acquired with negative electrospray
265 ionisation, and the full scan of mass-to-charge ratio (m/z) ranged from 100 to 1500.
266 Proteowizard software¹⁴ was used to convert the wiff files into mz XML files. Peak
267 peaking, noise filtering, retention time, m/z alignment, and feature quantification were
268 performed using apLCMS¹⁵. Three parameters were used to define a metabolite feature:
269 mass-to-charge ratio (m/z), retention time (min), and intensity values. Data were \log_2
270 transformed and only features detected in at least 50% of samples from one group were
271 used in further analyses. Missing values were imputed using half the mean of the feature
272 across all samples. Mummichog (version 2) was used for metabolic pathway enrichment
273 analysis (mass accuracy under 10 ppm)¹⁶.

274 **Acetylcholine measurement**

275 ACh was measured in heparinized plasma (SST[®] Gel Advance[®]; BD Diagnostics,
276 Franklin Lakes, NJ, USA) and in BAL using a commercially available
277 immunofluorescence kit (ab65345; Abcam, Cambridge, UK) according to the
278 manufacturer's instructions. Briefly, ACh was converted to choline by adding the enzyme
279 acetylcholinesterase to the reaction, which allows for total and free-choline measurement.
280 The amount of ACh present in the samples was calculated by subtracting the free choline

281 from the total choline. The products formed in the assay react with the choline probe and
282 can be measured by fluorescence with excitation and emission wavelengths of 535 and
283 587 nm, respectively (Paradigm Plate Reader; SpectraMax, San Diego, CA, USA). The
284 concentration of ACh was analysed using SoftMax[®] software (SpectraMax, Molecular
285 Devices, Sunnyvale, CA, USA), expressed as pmol.mL⁻¹.

286 **Soluble CD14 (sCD14) measurement**

287 Samples from heparinized plasma (SST[®] Gel Advance[®]; BD Biosciences, Franklin
288 Lakes, NJ, USA) were placed in 96-well plates. The concentration of sCD14 was
289 determined using an ELISA kit (DY383; R&D Systems, Minneapolis, MN, USA),
290 following the manufacturer's instructions, expressed as pg.mL⁻¹.

291 **Flow Cytometry**

292 Uncoagulated blood samples in EDTA-containing tubes (Vacutainer[®] EDTA K2; BD
293 Biosciences) were processed for flow cytometry analysis of circulating leukocytes.
294 Whole blood (1 mL) was separated and red blood cells were lysed using RBC lysis buffer
295 (Roche Diagnostics GmbH, Mannheim, GR). Leukocytes were washed in PBS containing
296 5% foetal bovine serum (FBS) (Gibco[™], USA), centrifuged, and resuspended in Hank's
297 balanced salt solution (Sigma-Aldrich, Merck, Darmstadt, Germany) containing 5% FBS,
298 followed by surface antigen staining. Similarly, cells obtained from BAL fluid were
299 processed for flow cytometry assays. Briefly, cells were stained with Fixable Viability
300 Stain 620 (1:1000) (BD Biosciences) and incubated with monoclonal antibodies specific
301 for CD14 (1:100) (M5E2; Biolegend), HLA-DR (1:100) (G46-6; BD Biosciences), CD16
302 (1:100) (3G8; Biolegend), and CD36 (1:100) (CB38, BD Biosciences) for 30 min at 4°C.
303 Stained cells were washed and fixed with BD Cytotfix[™] Fixation Buffer (554655; BD
304 Biosciences, San Diego, CA, USA). Data acquisition was performed using a LSR-

305 Fortessa™ flow cytometer (BD Biosciences, San Jose, CA, USA) and FACS-Diva
306 software (version 8.0.1) (BD Biosciences, Franklin Lakes, NJ, USA). For the analysis,
307 300,000 events were acquired for each sample. Data were evaluated using FlowJo®
308 software (version 10.7.0) (Tree Star, Ashland, OR, USA) to calculate the cell frequency,
309 dimensionality reduction, and visualisation using t-distributed stochastic neighbour
310 embedding. Gate strategy performed as described before ¹⁷, as shown in Figure S2.

311 **Cytokine Measurements**

312 The cytokines interleukin (IL)-6, IL-8, IL-1β, IL-10, and tumour necrosis factor
313 (TNF) were quantified in heparinized plasma and BAL fluid samples using a BD
314 Cytometric Bead Array (CBA) Human Inflammatory Kit (BD Biosciences, San Jose, CA,
315 USA), according to manufacturer's instructions. Briefly, after sample processing, the
316 cytokine beads were counted using a flow cytometer (FACS Canto TM II; BD
317 Biosciences, San Diego, CA, USA), and analyses were performed using FCAP Array
318 (3.0) software (BD Biosciences, San Jose, CA, USA). The concentrations of cytokines
319 were expressed as pg.mL⁻¹.

320 **Re-analysis of transcriptome data from lung biopsies of patients with Covid-19**

321 To gain a better understanding of the correlation between the altered concentrations
322 of ACh, AA, and AA-metabolites detected in the plasma and BAL fluid of severe/critical
323 Covid-19 patients, we performed a new analysis by re-using a previously published
324 transcriptome open dataset ¹⁸, deposited in the Gene Expression Omnibus repository
325 under accession no. GSE150316 ¹⁹. We used transcriptome data from lung samples
326 (n=46) from patients with Covid-19 (n=15), seven of which displayed a low viral load
327 and eight a high viral load, and non-Covid-19 patients (n=5) with other pulmonary
328 illnesses (negative control). Patients with a high viral load had meantime periods of

329 hospital stays (3.6 ± 2.2 days) and duration of illness (7.2 ± 3.02 days) shorter than the
330 patients with low viral load (14 ± 7.9 and 19 ± 4.9 days, respectively), as described by the
331 authors of the public data source ¹⁸. Hence, for analysis purposes, all patient samples were
332 grouped into four classifications: Covid-19 (CV), Covid-19 low viral load (CVL), Covid-
333 19 high viral load (CVH), and non-Covid-19 (NCV). The strategy for reanalysing the
334 transcriptome was implemented according to three consecutive steps: (i) co-expression
335 analysis, (ii) differential expression analysis, and (iii) biological network construction.
336 Initially, for the co-expression study, normalised transcriptome data in \log_2 of reads per
337 million (RPM) were filtered by excluding non-zero counts in at least 20% of the samples.
338 Next, the selected genes were explored in the R package Co-Expression Modules
339 identification Tool (CEMITool) ²⁰, using a p -value of 0.05 as the threshold for filtering.
340 Then, the co-expression modules were analysed for the occurrence of ACh and AA genes
341 list obtained from the Reactome pathways ²¹, as well as the Covid-19-related genes
342 obtained from the literature (Supplementary Appendix I). Next, differential gene
343 expression between samples from the lung biopsy transcriptome (CV, NCV, CVL, and
344 CVH) was measured using the DESeq2 package ²², with p -values adjusted using the
345 Benjamini and Hochberg method ²³. The list of differentially express genes (DEGs)
346 generated for all comparisons was filtered from the genes listed in Supplementary
347 Appendix I, considering the values of \log_2 of fold-change (FC) greater than 1
348 ($|\log_2(\text{FC})| > 1$) and adjusted $p < 0.05$. Finally, a first-order biological network was
349 constructed using co-expression module(s) containing genes associated with the ACh and
350 AA pathways to characterise the interplay between these mediators in combination with
351 Covid-19 severity markers, as well as to identify relevant DEGs and hub genes in this
352 network, using the BioGRID repository ²⁴. The networks were constructed, analysed, and
353 graphically represented using the R packages igraph ²⁵, Intergraph ²⁶, and ggnetwork ²⁷.

354 Due to the substantial influence of glucocorticoid treatment on the levels of some
355 mediators, we measured the sensitivity of genes from the differential expression analysis
356 between CV samples from patients who underwent treatment (CTC, three patients and
357 ten samples) and patients who were not treated (NCTC, 12 patients and 36 samples), as
358 previously described ¹⁸.

359 **Statistical Analysis**

360 Two-tailed tests were used for the statistical analysis, with a significance value of
361 $p < 0.05$ and a confidence interval of 95%. The data were evaluated for a normal
362 distribution using the Kolmogorov–Smirnov test. The parametric data were analysed
363 using unpaired t-tests (for two groups) or one-way ANOVA followed by Tukey’s multiple
364 comparison tests for three or more groups simultaneously. For data that did not display a
365 Gaussian distribution, Mann-Whitney (for two-group comparisons) or Kruskal-Wallis
366 testes were used, followed by Dunn’s post-tests for analysis among three or more groups.
367 The cytokine network data in patients with Covid-19 were analysed using significant
368 Spearman’s correlations at $p < 0.05$. Data were represented by connecting edges to
369 highlight positive strong ($r \geq 0.68$; thick continuous line), moderate ($0.36 \geq r < 0.68$;
370 thinner continuous line), or weak ($0 > r < 0.36$; thin continuous line) and negative strong
371 ($r \leq -0.68$; thick dashed line), moderate ($-0.68 > r \leq -0.36$; thinner dashed line), or weak
372 ($-0.36 < r > 0$; thin dashed line), as proposed previously ^{28,29}. The absence of a line
373 indicates the non-existence of the relationship. The Venn diagrams were elaborated using
374 the online tool Draw Venn Diagram (<http://bioinformatics.psb.ugent.be/webtools/Venn/>).
375 The results were tabulated using GraphPad Prism software (version 8.0) and the
376 differences were considered statistically significant at $p < 0.05$. See the Additional
377 Statistical Report section for more information. Some of the confounding variables
378 associated with Covid-19 (age, sex, obesity, hypertension, and diabetes mellitus) were

379 analysed for their potential impacts on the main analytical procedures of this study, such
380 as ACh, AA, 5-HETE, and 11- HETE measurements of the plasma (healthy,
381 asymptomatic-to-mild, moderate, severe, and critical patients) and BAL (severe and
382 critical patients) samples. This analysis was performed using the Kruskal-Wallis, Mann-
383 Whitney, Spearman's correlation, or Chi-square (χ^2) tests (Table S7-S9).

384 **Results**

385 **Study Population**

386 This study enrolled 39 healthy-participants, 13 hospitalized non-Covid-19, and
387 190 Covid-19 patients aged 16-96 years from April to November 2020. The 190 Covid-
388 19 patients were categorized as having asymptomatic-to-mild (n=43), moderate (n=44),
389 severe (n=54), or critical (n=49) disease (Table S2).

390 **Covid-19 Modifies Circulating Soluble Mediators and Cell Populations**

391 To determine whether SARS-CoV-2 infection alters the metabolism of lipid
392 mediators, we used high-resolution sensitive mass spectrometry to perform targeted
393 eicosanoid analysis and nontargeted metabolomics using plasma from healthy-
394 participants and Covid-19 patients. In total, 8,791 metabolite features were present in at
395 least 50% of all samples, and the relative abundance of 595 metabolite features (FDR
396 adjusted $P < 0.05$) was altered in the groups studied (Figure 1A). Two-way hierarchical
397 clustering based on these significant metabolite features resulted in three clear clusters:
398 one for severe/critical Covid-19 patients, one for healthy-participants and one for
399 asymptomatic-to-mild and moderate Covid-19 (Figure S1A). Pathway analysis revealed
400 the top significant metabolic pathways to be enriched in features involved in fatty acid
401 biosynthesis, metabolism, activation, and oxidation (Figure 1B). Compared to healthy-

402 participants, tentative metabolite annotations suggested an increased abundance of fatty
403 acids (FFAs), such as linoleic acid, tetradecanoate, dodecanoate and AA, in COVID-19
404 (Figure 4C-F). Among the identified lipids, AA was the most abundant, and its levels
405 correlated with the severity of Covid-19 (Figure 1F). Linoleic acid can be metabolized to
406 AA, which in turn is a substrate for eicosanoids, such as 5-hydroxyeicosatetraenoic acid
407 (5-HETE) and 11-hydroxyeicosatetraenoic acid (11-HETE) (Figure 1G, 1H); both
408 molecules with function in the immune response. Overall, the increased plasma levels of
409 AA in Covid-19 indicate that it predicts disease severity.

410 As eicosanoids induce cell recruitment and regulate immune responses, we next
411 determined the profile of immune cells and soluble mediators in whole blood and plasma
412 of patients with Covid-19 and healthy-participants. According to whole-blood analysis,
413 absolute leukocyte and neutrophil counts (Figure 2A, 2B) were significantly higher but
414 lymphocyte counts (Figure 2C) significantly lower in patients with severe/critical disease
415 than in those with moderate disease. Eosinophil (Figure 2D) and basophil counts (Figure
416 2E) were reduced severe disease compared to asymptomatic and moderate disease.

417 Although no differences in total monocyte counts among the groups (Figure 2F)
418 were observed based on CD16, CD14 and HLA-DR, expression of membrane CD14 was
419 reduced in all SARS-CoV-2-infected patients compared to healthy-participants (Figure
420 2G; Figure S2, S3). In parallel, CD36 expression was decreased in monocytes from
421 patients with severe/critical disease (Figure 2H), but sCD14 was increased only in plasma
422 from critical patients (Figure 2I). We did not detect differences in classic or non-classic
423 monocytes, but the percentage of intermediate monocytes was decreased in all SARS-
424 CoV-2-infected participants compared to healthy-participants (Figure 2J, 2K, 2L). Based
425 on plasma cytokine level analysis, patients with moderate, severe, and critical disease

426 share a Covid-19 cytokine profile defined by increased IL-8, IL-6, and IL-10 (Figure 2M,
427 2N, 2Q) levels, with unaltered IL-1 β and TNF levels (Figure 2O, 2P).

428 **Covid-19 Induces Strong Lung Responses**

429 We performed measurements of BAL from hospitalized Covid-19 and non-
430 Covid-19 patients. Changes in lung metabolomics induced by SARS-CoV-2 infection
431 (Figure 3A; Figure S1B) included alterations in sphingolipids, beta oxidation of
432 trihydroxyprostanoid-CoA, biosynthesis and metabolism of steroidal hormones, vitamin
433 D3, and glycerophospholipids (Figure 3B). We also evaluated AA and its metabolites.
434 Despite no differences in AA, levels of 5-HETE and 11-HETE in BAL were significantly
435 higher in Covid-19 than in non-Covid-19 patients, though other metabolites did not differ
436 between these groups (Figure 3C). When assessing leukocytes in BAL between the
437 patient groups, we found no differences in total or differential counts, with the exception
438 of lymphocyte numbers (Figure 3D, 3E). In contrast to eicosanoids, cytokine profiles in
439 Covid-19 and non-Covid-19 patients were similar (Figure 3F), suggesting that lipid
440 mediators contribute to the pathophysiological processes induced by SARS-CoV-2.
441 Interestingly, we observed a significant reduction in classical (Figure 3G) and
442 intermediate (Figure 3H) monocytes in BAL from Covid-19 patients. In parallel, CD14
443 and CD36 expression in monocyte was lower in BAL of Covid-19 than in that of non-
444 Covid-19 patients (Figure 3I, 3J).

445 **Acetylcholine, Cytokines and Eicosanoids are Higher in the Lung Micro- 446 Environment**

447 We compared systemic and lung responses only in patients with severe/critical
448 Covid-19 and found significantly higher levels of cytokines in BAL than in blood (Figure
449 4A). When comparing lipid mediator levels in either compartment from the same Covid-

450 19 patients, we detected lower AA but higher levels of 5-HETE and 11-HETE in BAL
451 than in blood (Figure 4B, 4C, 4D). Previous results from our group³ have shown that
452 eicosanoids contribute to ACh release. Therefore, we next measured ACh in patients with
453 Covid-19 and observed higher plasma levels of ACh in patients with Covid-19; in
454 addition, ACh was elevated in patients with severe/critical disease compared with those
455 with asymptomatic/moderate disease or healthy-participants (Figure 4E). Unexpectedly,
456 in patients with severe/critical Covid-19, ACh levels in BAL were 10-fold higher than
457 those in serum, and patients treated with glucocorticoids showed decreases in ACh in
458 both compartments (Figure 4F, 4G). Interesting, neutrophil counts were higher in BAL,
459 as these cells produce high levels of 5-HETE and IL-1 β , both of which are mediators of
460 ACh release^{30,31} (Figure 4H). Correlation analysis was then performed to evaluate the
461 relationship between eicosanoids, cytokines, sCD14 and ACh in patients with Covid-19.
462 When comparing blood samples from all patients, we detected strong correlations
463 between ACh *versus* IL-1 β and moderate correlations between ACh *versus* AA. A
464 substantial number of interactions between AA and its metabolites and between cytokines
465 and eicosanoids were observed (Figure 4I; Figure S4A). Correlations among all
466 parameters were also observed in BAL (Figure 4J; Figure S4B). To evaluate the benefit
467 of glucocorticoid treatments and their relationship with eicosanoids, CD14 and ACh, we
468 analysed the intersections in a Venn diagram of blood and BAL from severe/critical
469 Covid-19. The results showed that treatment of Covid-19 with glucocorticoids did not
470 have a significant influence on eicosanoid or sCD14 release in patients with more severe
471 stages of disease; in critical patients, however, reductions of 44% and 65% in ACh levels
472 in blood and BAL, respectively, were observed (Figure 4K-4Q; Figure S5). These
473 findings suggest that the use of glucocorticoids has a positive effect on resolution of the

474 inflammatory process because they reduce ACh release, which directly or indirectly
475 stimulates cell recruitment and proinflammatory mediator release.

476 **Altered Expression of Acetylcholine and Arachidonic Acid Pathway Genes in Lung**
477 **Biopsies From Some Covid-19 Patients**

478 In this study, we reanalysed the lung biopsy transcriptome from Covid-19 patients
479 to evaluate expression of ACh and AA pathway genes (Supplementary Appendix I).
480 These genes were coexpressed only in a single module (M1) that included genes related
481 to the ACh release cycle, AA metabolism, cholinergic and eicosanoid receptors, and
482 biomarkers of Covid-19 severity (Figure 5A; Table S4; Supplementary Appendix II).
483 Furthermore, expression of nearly all genes was upregulated in some deceased Covid-19
484 patients with long hospital stays and low viral loads (Figure 5B; Figure S6A;
485 Supplementary Appendix III). These differentially expressed genes populated the
486 biological network and are likely under the action of some hubs (Figure 5C;
487 Supplementary Appendix IV), such as oestrogen receptor II (ESR2) and albumin (ALB).
488 We identified a unique proinflammatory gene expression profile in lung biopsies related
489 to cholinergic and eicosanoid receptors (Figure 5H, 5I; Figure S6B, S6C). In combination
490 with the altered levels of ACh, AA, and AA metabolites found in patient from our cohort,
491 the transcriptome data reported herein strengthen the likelihood that these mediators
492 contribute to Covid-19 severity (Figure 5D-5G). Interestingly, lung samples from Covid-
493 19 patients with short hospital stays and high viral loads did not present this unique
494 expression profile of ACh or AA pathway genes (Figure 5H, 5I; Figure S6B, S6C). Some
495 Covid-19 patients treated versus not with glucocorticoid showed transcript expression of
496 monoglyceride lipase (MGLL) and N-acylethanolamine acid amidase (NAAA) and up-
497 regulation of fatty acid amide hydrolase (FAAH), which are involved in the production
498 of AA from endocannabinoid (cases 3, 9, and 11; Figure 5B; Supplementary Appendix

499 III). Besides, we detected other DEGs in biopsy samples from Covid-19 patients
500 (glucocorticoid-treated versus non-treated) associated with AA, ACh, interferon
501 pathways, and Covid-19 biomarkers (Supplementary Appendix III).

502 **Discussion**

503 A consensus is building around the fatal effects of SARS-CoV-2 infection, which is
504 increasingly believed to cause death as a result of systemic hyperinflammation and multi-
505 organ collapse³², secondary to systemic cytokine storms³³⁻³⁵. However, few studies have
506 compared pulmonary and systemic inflammation³⁶ or considered the contribution of
507 eicosanoids and neurotransmitters to these effects. In our study, we hypothesised that, in
508 Covid-19, pulmonary cells and leukocytes, in addition to cytokines, release eicosanoids
509 and ACh, mediating local and systemic manifestations. In patients with severe/critical
510 SARS-CoV-2 infection, we found that ACh, 5-HETE, 11-HETE, and cytokines were
511 more abundant in the lung than under systemic conditions. In contrast, only the levels of
512 AA were found to be higher in the circulation than in the BAL fluid. Interestingly, in
513 patients with severe/critical disease who were treated with corticosteroids, only ACh was
514 inhibited.

515 In our study, we compared the lung and systemic responses in association with the
516 lung transcriptome and demonstrated a robust correlation between lipid mediators,
517 neurotransmitters, and their receptors in SARS-CoV-2 infection. However, contrary to
518 what has been suggested by previous studies^{37,38}, only small amounts of eicosanoids were
519 found in the plasma of patients with severe/critical disease, with significant differences
520 observed only in AA, 5-HETE, and 11-HETE. Interestingly, the levels of 5-HETE and
521 11-HETE were found to be remarkably higher in BAL, as well as AA in plasma,
522 suggesting that AA and its metabolites mediate responses to Covid-19. 5-HETE induces

523 neutrophil recruitment ³⁹, pulmonary oedema ⁴⁰, and ACh release ³⁰. It is released by
524 human neutrophils, and its esterified form promotes IL-8 secretion ³¹. Unlike the
525 esterified form ³¹, free-5-HETE did not inhibit NETs formation, a key event in Covid-19
526 ⁴¹. Remarkably, 11-HETE originating from monocytes/macrophages ⁴², endothelial cells
527 ⁴³, and platelets ⁴⁴ is induced by hypoxia ⁴⁵, IL-1 β ⁴⁶, contributes to ACh functions ⁴³, and
528 inhibits insulin release ⁴⁷. The involvement of AA was confirmed by bioinformatic
529 analyses that identified the expression or upregulation of genes related to AA metabolism
530 and eicosanoid receptors in some lung biopsies. These included the OXER1 gene, which
531 encodes a receptor for AA and 5-HETE ⁴⁸ which mediates neutrophil
532 activation/recruitment ^{49,50}. Our metabolomic analysis also showed an increase in the
533 plasma AA and linoleic acid levels, similar to a plasma lipidome performed by Schwarz
534 et al., suggesting a strong correlation between lipid mediators and Covid-19 severity ⁵¹.
535 Accordingly, the ELOVL2 gene, which is involved in linoleic acid metabolism and AA
536 synthesis ⁵², was upregulated in lung biopsies.

537 The RNA expression of ALOX5, an enzyme that participates in lipid mediator
538 production, is upregulated in some immune cell types from severe Covid-19 patients ⁵³,
539 and has been detected in the lung biopsies of deceased Covid-19 patients ¹⁸. In contrast
540 to our lung transcriptome re-analysis findings, the expression of cytochrome p450 (CYP)
541 enzymes, which are also involved in lipid mediator generation, was not detected in the
542 peripheral blood mononuclear cells (PBMC) transcriptome re-analysis from severe
543 Covid-19 patients ⁵³. One possible explanation for this contradiction is that Covid-19 is a
544 heterogeneous illness composed of distinct tissue gene expression associated with Covid-
545 19 severity and different immunopathological profiles in infected tissues ^{18,54}. This
546 immunological heterogeneity could be related to two types of evolution of severe Covid-
547 19 patients, one associated with a high viral load and susceptibility to SARS-CoV-2

548 infection, a shorter hospitalisation time, and exudative diffuse alveolar damage, and
549 another associated with a low or undetectable viral load, a mixed lung histopathological
550 profile, and a longer hospitalisation time associated with non-homeostatic pulmonary
551 inflammation^{18,54,55}. In this context, we found that the expression levels of some lipid
552 mediators and ACh and AA pathway genes varied in the plasma and BAL samples of
553 severe/critical patients, which were found to be preferentially activated in the lungs of
554 deceased Covid-19 patients with low viral loads, long hospitalisation times, and
555 damaging lung inflammation.

556 Nevertheless, it remains unclear whether AA and linoleic acid contribute to host
557 protection⁵⁶ and tissue damage, or whether they represent a viral escape mechanism. AA
558 is known to directly interact with the virus, reducing its viability and inducing membrane
559 disturbances, disfavours SARS-CoV-2 entry⁵⁷⁻⁵⁹. On the other hand, reduced plasma
560 AA levels may be associated with lung injury and poor outcomes in Covid-19 infection
561⁶⁰. Within this context, Shen and et al. found lower concentrations of AA in survivors of
562 severe Covid-19 infection³⁷. However, in the present study, the levels of AA were found
563 to be increased in the plasma of patients who died from severe Covid-19, suggesting that
564 the potential benefits of AA are overcome by a higher production of its proinflammatory
565 metabolites, 5-HETE and 11-HETE. Interestingly, in our cohort, AA, 5-HETE, and 11-
566 HETE were not altered in the plasma or BAL fluid of patients with severe/critical Covid-
567 19 infection who had received glucocorticoid treatment. This may be explained by the
568 fact that AA, in addition to calcium-activated-PLA₂⁶¹ also originates from
569 glucocorticoid-insensitive phospholipase⁶², adipocyte destruction⁶³, linoleic acid⁶⁴, or
570 the degradation of endocannabinoids by FAAH⁶⁵, a macrophage enzyme detected in
571 SARS-CoV-2-infected patients⁶⁶. Notably, some CVL Covid-19 patients, regardless of
572 whether they were treated or not with glucocorticoids, showed transcript expression of

573 MGLL and NAAA, as well as an up-regulation of FAAH and all of the enzymes involved
574 in the production of AA from endocannabinoid ⁶⁷. In addition, we detected other DEGs
575 in biopsy samples (glucocorticoid-treated versus non-treated) associated with AA, ACh,
576 interferon pathways, and Covid-19 biomarkers. Glucocorticoids have been used widely
577 to reduce the morbidity and mortality rates of Covid-19 patients, but have not been
578 effective for all patients ⁶⁸. The mortality rate for glucocorticoid-treated hospitalised
579 Covid-19 patients from our cohort was higher than that reported in the RECOVERY trial
580 and similar to that described in the CoDEX trial conducted in Brazil ⁶⁹. High mortality
581 rates could be associated with several factors, including a low mean PaO₂:FiO₂ ratio and
582 overloaded public health systems in countries with limited resources, such as Brazil ⁶⁹
583 and as well as glucocorticoid dose, initiation, and duration of therapy ^{70,71}. In addition,
584 the precise threshold at which a patient should be treated with glucocorticoids, that is to
585 avoid the manifestation of adverse effects associated with comorbidities and inefficient
586 clearance of SARS-CoV-2, remains unclear ⁷². However, a delayed start of glucocorticoid
587 therapy could result in a lack of response due to patients reaching a point of no return, as
588 suggested previously by our research group with regards to scorpion poisoning, which
589 triggers a sterile inflammatory process ³. On the other hand, considering that Covid-19 is
590 a non-sterile hyperinflammatory disease, the administration of glucocorticoids is more
591 effective after the initial phase in which hospitalised patients have low or undetectable
592 viral loads ^{18,68}. Our data suggest that SARS-CoV-2 infection activates the glucocorticoid-
593 insensitive release of AA metabolites associated with Covid-19 severity. Hence, lipid
594 mediator production pathways could be important molecular targets for Covid-19
595 treatment, as suggested by other researchers ⁵³. Accordingly, we suggested that, in order
596 to improve the benefits of glucocorticoid therapy in hospitalized patients, who show

597 lower or undetectable viral loads, patients should be treated as soon as possible in
598 combination with AA metabolism inhibitors.

599 CD36 is expressed in several cells ^{73,74}, where it induces Ca⁺⁺ mobilisation, cell
600 signalling, LTB₄ production, and cellular fatty acid uptake ⁷⁵⁻⁷⁸. The maintenance of high
601 free-AA levels in patients with severe/critical glucocorticoid-treated disease may result
602 from the reduction of CD36 on macrophage membranes. Intriguingly, CD36 is a gustatory
603 lipid sensor ⁷⁹, whose deficit in cell membranes may account for the symptoms of ageusia,
604 anosmia, diarrhoea, hyperglycaemia, platelet aggregation, and cardiovascular
605 disturbances experienced by Covid-19 patients ⁷⁵⁻⁷⁷. CD36 is a substrate of matrix
606 metalloproteinase-9 (MMP-9) and disintegrin metalloproteinase domain-containing
607 protein 17 (ADAM17) ^{80,81}. Decreased CD36 expression in Covid-19 patients most likely
608 results from the action of these enzymes. MMP-9 is produced by neutrophils ⁸², induced
609 by TNF- α ⁸³, unaffected by glucocorticoids, and associated with respiratory syndrome in
610 Covid-19 ⁸⁴. ADAM17 has been described as a target for Covid-19 treatment ⁸⁵.

611 In agreement with previous reports ^{1,34,86,87}, in the present study, high
612 concentrations of IL-6, IL-8, and IL-10 were detected, along with insignificant levels of
613 IL-1 β in plasma. In contrast, the inflammatory cytokine TNF- α was found at the lowest
614 concentration in BAL fluid, and insignificant levels were detected in the blood. The low
615 levels of TNF- α production are correlated with the decreased counts of intermediate
616 monocytes in the blood and BAL, which are major sources of this cytokine ⁸⁸. As
617 expected, in the BAL from patients with severe/critical Covid-19, the levels of IL-8, IL-
618 6, IL-1 β , TNF- α , and IL-10 were significantly higher compared with the plasma of all
619 participants, or when paired with patients' own plasma. Notably, in BAL, the most
620 abundant cytokine was IL-8, which is produced by neutrophils ⁸⁹, lung macrophages ⁹⁰,
621 and bronchial epithelial cells ¹⁰, and is induced by 5-HETE ³¹ and ACh ¹⁰. Interestingly,

622 BAL fluid from non-Covid-19 patients also presented a high concentration of cytokines
623 that did not differ from that of patients with Covid-19. This suggests that cytokine storms
624 are not a key differential factor in this disease. Contrary to our expectations,
625 glucocorticoids did not alter cytokine production (Table S7). As a result, we suggest that,
626 regardless of whether Covid-19 is treated with glucocorticoids, cross-talk occurs between
627 cytokines, lipid mediators, and ACh, as previously reported ^{2,3,91}. IL-1 β induces 11-HETE
628 ⁴⁶; arterial relaxation induced by ACh is mediated by 11-HETE and is inhibited by
629 indomethacin ⁴³. In our studies on scorpion envenomation, ACh release was found to be
630 mediated by PGE₂-induced by IL-1 β and inhibited by indomethacin ³. In the present
631 study, comparing AA, 5-HETE, 11-HETE, cytokine, and receptor expression
632 demonstrated the absence of glucocorticoid effects. These results, in addition to the
633 results of other studies from our laboratory ³, suggest that glucocorticoids did not have an
634 effect in our cohort. This was most likely due to the fact that treatment was started late,
635 namely after inflammation has been triggered by infection. In this context, Covid-19
636 patients could have already reached the point of no return, similar to what has been
637 previously described in scorpion envenomation ³.

638 As predicted by Virgilis and Giovani ⁹², neurotransmitters are produced in Covid-
639 19. ACh induces mucus secretion, bronchoconstriction, lung inflammation and
640 remodelling ⁹, cardiac dysfunction in scorpionism ³, NETs formation ⁹³, IL-8 release ¹⁰,
641 thrombosis ⁹⁴, and obesity-related severity ⁹⁵. In addition to the nervous system ⁴, ACh is
642 also produced by pulmonary vessels ⁹⁶, airway epithelial cells ⁶, and immune cells ⁵. When
643 binding to anti-inflammatory neural nicotinic receptors induces AA release ⁹⁷, it inhibits
644 nicotine receptors ⁹⁷, which are highly expressed in lungs ⁹⁸. In our cohort, a correlation
645 between the AA and ACh levels and the severity of Covid-19 infection was observed,
646 which was reinforced by the results of our bioinformatics study. Our lung transcriptome

647 re-analyses showed that ACh release cycle genes were activated, including acetylcholine-
648 synaptic release (synaptotagmin 1) and neuronal choline transporter (Solute Carrier
649 Family 5 Member 7, SLC5A7). Accordingly, SLC5A7 gene expression was higher in the
650 lung of patients who died from Covid-19 infection than patients who survived⁹⁹. Because
651 this gene mediates the translocation of choline into lung epithelial cells¹⁰⁰ and
652 macrophages¹⁰¹, the production of ACh in BAL may also depend on non-neuronal cells.
653 Indeed, the ACh repressor gene in non-neural cells (RE1 Silencing Transcription Factor)
654 is reduced in the lungs of patients who died of Covid-19⁹⁹. The activation of T-
655 lymphocyte EP4 induces the release of ACh¹⁰², suggesting that AA metabolites
656 contribute to the release of ACh from lung and immune cells. As expected, ACh
657 production in patients with severe/critical disease was found to be inhibited by
658 glucocorticoids, since this drug blocks ACh production by lung epithelial cells^{103–105}.
659 Patients with Covid-19 (mostly methylprednisolone-treated patients) showed lower
660 plasma levels of choline and higher plasma levels of phosphocholine³⁷. In addition, a
661 distinct pattern of ACh receptor mRNA expression was found in patients who died of
662 Covid-19 (mainly in the CVL-lengthy hospital stay group). This profile is characterised
663 by low levels of expression of the nicotinic receptor encoded by cholinergic receptor
664 nicotinic alpha 7 subunit gene (CHRNA7) and increased levels of expression of two
665 nicotinic and one muscarinic receptor in deceased-CVL compared to deceased non-
666 Covid-19 patients. These proteins are encoded by the cholinergic nicotinic alpha 3 subunit
667 gene (CHRNA3), the cholinergic nicotinic receptor 5 subunit gene (CHRNA5), and the
668 muscarinic cholinergic receptor 3 gene (CHRM3), respectively. These three upregulated
669 genes were also co-expressed and associated with pulmonary inflammatory disorders
670^{9,106–110}. Notably, SARS-CoV-2 spike glycoprotein interacts with the $\alpha 7$ nicotinic

671 acetylcholine receptor, which may compromise the cholinergic anti-inflammatory
672 pathway¹¹¹.

673 The ACh-nicotinic receptor, encoded by CHRNA7, is expressed in various lung
674 cells and macrophages¹¹². It displays extensive anti-inflammatory activities, including
675 the inhibition of pro-inflammatory cytokine production¹¹³, the recruitment of neutrophils
676¹¹⁴, and the reduction of CD14 expression in human monocytes¹¹⁵. The increased degrees
677 of inflammation in the BAL fluid of patients with severe/critical Covid-19 may be
678 associated with the lower levels of anti-inflammatory CHRNA7 expression. However, a
679 reduction in monocyte CD14 may result from high levels of IL-6 production¹¹⁶, since the
680 levels of CHRNA7 expression were very low. Interestingly, the ACh-M3 receptor in
681 immune cells has been found to be up-regulated by ACh, which mediates its pro-
682 inflammatory actions, including the production of IL-8 and the recruitment of neutrophils
683¹¹⁷. Furthermore, the interaction between ACh and its receptor triggers the AA-derived
684 release of eicosanoids, including 5-HETE^{97,118,119}. Remarkably, vitamin D modulates the
685 ACh-M3 receptor¹²⁰, which may explain its beneficial effects in the prevention of Covid-
686 19¹²¹. Based on the anti-inflammatory effects of nicotinic receptors and the
687 downregulation of the SARS-CoV-2 receptor ACE2 promoted by nicotine, therapies
688 involving nicotinic receptors have been proposed to treat Covid-19 infection^{122,123}. In
689 fact, based on these findings, an acetylcholinesterase inhibitor^{124,125} and a nicotinic
690 receptor agonist have been tested^{126,127}. However, recent studies have demonstrated that
691 nicotine and smoking increase ACE2 receptor density^{128,129}, and that the potential
692 beneficial effects of nicotine were restricted to a small group of individuals¹³⁰. Our
693 findings provide a warning that precautions should be taken when considering the
694 therapeutic use of nicotinic agonists, since patients with severe/critical Covid-19 were
695 found to release high amounts of ACh, in addition to showing increased levels of M3-

696 receptor expression. Due to the antiviral and anti-inflammatory effects of AA, it has been
697 proposed to treat Covid-19 patients ⁶⁰. Nevertheless, AA may be not be an adequate
698 therapeutic target, based on both our findings and previous studies ¹³¹, which have shown
699 that AA can favour hyperinflammation and lethality in Covid-19 infection. In conclusion,
700 ACh, AA, 5-HETE, and 11-HETE mediate the innate immune response to SARS-CoV-2
701 and may define the outcome of infection.

702 Covid-19 severity can be associated with disruption of homeostatic lipidome and
703 metabolic alterations and this phenomenon may be influenced by comorbidities/risk
704 factors related to the infection. Our findings demonstrated that (i) high plasma levels of
705 ACh and lipid mediators positively correlated with Covid-19 severity; and (ii) only
706 hypertension and/or age were confounding variables for analyzing the association of high
707 plasma levels of AA, 5-HETE, and ACh with disease severity (Table S7). Similarly, the
708 correlation between altered plasma profile of lipid mediators and Covid-19 severity is
709 associated with selective comorbidities – mainly high body mass index (BMI) – but
710 poorly associated with gender, advanced age, and diabetes. However, the correlation
711 between altered AA and/or 5-HETE levels and disease severity is associated with male
712 gender, hypertension, and heart disease, but not BMI⁵³.

713 We also examined whether glucocorticoid-therapy interfered with the potential
714 effect of some confounding variables on the correlation between high ACh levels and
715 Covid-19 severity in severe/critical patients. Despite the relatively underrepresented
716 samples from non-glucocorticoid treated patients, no confounding variable significantly
717 affected the correlation between plasma and BAL ACh levels and Covid-19 severity in
718 severe/critical patients treated or not with glucocorticoids (Table S8). The altered plasma
719 and BAL levels of the lipid mediators AA, 5-HETE, and 11-HETE in severe/critical
720 patients were associated with the disease severity but not with the confounding variables

721 tested (Table S9). Altogether, the findings here reported suggest that age and/or
722 hypertension are significant confounding variables for analyzing the association between
723 increased levels of cholinergic and lipid mediators and Covid-19 severity. Also, the
724 confounding variables tested probably did not modify the inhibitory action of
725 glucocorticoids on plasma and BAL ACh levels in severe/critical patients.

726 To the best of our knowledge, this study is the first to demonstrate that the lung
727 inflammatory process and poor outcomes of patients with Covid-19 infection are
728 associated with high levels of lipid mediators and ACh, produced via a partially
729 glucocorticoid-insensitive pathway. Glucocorticoid therapy was found to lower only the
730 levels of ACh. Thus, to improve the benefits of glucocorticoid therapy, we suggest that
731 treatment in hospitalised patients be started early and be preferentially administered to
732 patients with low or undetectable viral loads and harmful lung inflammation in
733 combination with AA metabolism inhibitors.

734 **Conclusions**

735 We demonstrate for the first time that the lung inflammatory process and worse
736 outcomes in Covid-19 are associated with lipid mediators and ACh, which are produced
737 through a partially glucocorticoid-insensitive pathway. To improve the benefits of
738 glucocorticoid therapy, we suggest that it should be started early in severe/critical
739 hospitalized patients and in combination with AA metabolism inhibitors.

740

741

742

743 **References**

- 744 1. Huang C, Wang Y, Li X, et al. Clinical features of patients infected with 2019
745 novel coronavirus in Wuhan, China. *Lancet* 2020;395(10223):497–506.
- 746 2. Esser-von Bieren J. Immune-regulation and -functions of eicosanoid lipid
747 mediators. *Biol. Chem.* 2017;
- 748 3. Reis M, Rodrigues F, Lautherbach N, et al. Interleukin-1 receptor-induced PGE2
749 production controls acetylcholine-mediated cardiac dysfunction and mortality
750 during scorpion envenomation. *Nat Commun* 2020;11(1).
- 751 4. McGovern AE, Mazzone SB. Neural regulation of inflammation in the airways
752 and lungs. *Auton Neurosci Basic Clin* 2014;
- 753 5. Wessler I, Kirkpatrick CJ. Cholinergic signaling controls immune functions and
754 promotes homeostasis. *Int. Immunopharmacol.* 2020;
- 755 6. Proskocil BJ, Sekhon HS, Jia Y, et al. Acetylcholine is an autocrine or paracrine
756 hormone synthesized and secreted by airway bronchial epithelial cells.
757 *Endocrinology* 2004;
- 758 7. Chang EH, Chavan SS, Pavlov VA. Cholinergic control of inflammation,
759 metabolic dysfunction, and cognitive impairment in obesity-associated disorders:
760 Mechanisms and novel therapeutic opportunities. *Front. Neurosci.* 2019;
- 761 8. Roy A, Guatimosim S, Prado VF, Gros R, Prado MAM. Cholinergic activity as a
762 new target in diseases of the heart. *Mol Med* 2014;
- 763 9. Kistemaker LEM, Gosens R. Acetylcholine beyond bronchoconstriction: roles in
764 inflammation and remodeling. *Trends Pharmacol Sci* 2015;36(3):164–71.
- 765 10. Profita M, Bonanno A, Siena L, et al. Acetylcholine mediates the release of IL-8
766 in human bronchial epithelial cells by a NFkB/ERK-dependent mechanism. *Eur J*
767 *Pharmacol* 2008;

- 768 11. Shields MD, Riedler J. Bronchoalveolar lavage and tracheal aspirate for
769 assessing airway inflammation in children. *Am J Respir Crit Care Med*
770 2000;162(2 II).
- 771 12. Schindelin J, Rueden CT, Hiner MC, Eliceiri KW. The ImageJ ecosystem: An
772 open platform for biomedical image analysis. *Mol Reprod Dev* 2015;82(7–
773 8):518–29.
- 774 13. Sorgi CA, Peti APF, Petta T, et al. Data descriptor: Comprehensive high-
775 resolution multiple-reaction monitoring mass spectrometry for targeted
776 eicosanoid assays. *Sci Data* 2018;
- 777 14. Chambers MC, MacLean B, Burke R, et al. A cross-platform toolkit for mass
778 spectrometry and proteomics. *Nat. Biotechnol.* 2012;
- 779 15. Yu T, Park Y, Johnson JM, Jones DP. apLCMS-adaptive processing of high-
780 resolution LC/MS data. *Bioinformatics* 2009;
- 781 16. Li S, Park Y, Duraisingham S, et al. Predicting Network Activity from High
782 Throughput Metabolomics. *PLoS Comput Biol* 2013;
- 783 17. Kuri-Cervantes L, Pampena MB, Meng W, et al. Comprehensive mapping of
784 immune perturbations associated with severe COVID-19. *Sci Immunol* 2020;
- 785 18. Desai N, Neyaz A, Szabolcs A, et al. Temporal and spatial heterogeneity of host
786 response to SARS-CoV-2 pulmonary infection. *Nat Commun [Internet]*
787 2020;11(1):6319. Available from: [http://www.nature.com/articles/s41467-020-](http://www.nature.com/articles/s41467-020-20139-7)
788 20139-7
- 789 19. Edgar R, Domrachev M, Lash AE. Gene Expression Omnibus: NCBI gene
790 expression and hybridization array data repository. *Nucleic Acids Res* 2002;
- 791 20. Russo PST, Ferreira GR, Cardozo LE, et al. CEMiTool: A Bioconductor package
792 for performing comprehensive modular co-expression analyses. *BMC*

- 793 Bioinformatics 2018;
- 794 21. Jassal B, Matthews L, Viteri G, et al. The reactome pathway knowledgebase.
795 Nucleic Acids Res 2020;
- 796 22. Love MI, Huber W, Anders S. Moderated estimation of fold change and
797 dispersion for RNA-seq data with DESeq2. Genome Biol 2014;
- 798 23. Benjamini Y, Hochberg Y. Controlling the False Discovery Rate: A Practical and
799 Powerful Approach to Multiple Testing. J R Stat Soc Ser B 1995;
- 800 24. Stark C, Breitkreutz BJ, Reguly T, Boucher L, Breitkreutz A, Tyers M.
801 BioGRID: a general repository for interaction datasets. Nucleic Acids Res 2006;
- 802 25. Csardi G, Nepusz T. The igraph software package for complex network research.
803 InterJournal Complex Syst 2006;
- 804 26. Maintainer MB, Bojanowski M. Package “intergraph” Type Package Title
805 Coercion Routines for Network Data Objects. 2016;
- 806 27. Tyner S, Briatte F, Hofmann H. Network visualization with ggplot2. R J
807 2017;9(1):27–59.
- 808 28. Taylor R. Interpretation of the Correlation Coefficient: A Basic Review. J
809 Diagnostic Med Sonogr 1990;
- 810 29. Abreu-Filho PG, Tarragô AM, Costa AG, et al. Plasma Eicosanoid Profile in
811 Plasmodium vivax Malaria: Clinical Analysis and Impacts of Self-Medication.
812 Front Immunol 2019;
- 813 30. Fukunaga Y, Mine Y, Yoshikawa S, Takeuchi T, Hata F, Yagasaki O. Role of
814 prostacyclin in acetylcholine release from myenteric plexus of guinea-pig ileum.
815 Eur J Pharmacol 1993;233(2–3):237–42.
- 816 31. Clark SR, Guy CJ, Scurr MJ, et al. Esterified eicosanoids are acutely generated
817 by 5-lipoxygenase in primary human neutrophils and in human and murine

- 818 infection. *Blood* 2011;
- 819 32. Chen G, Wu D, Guo W, et al. Clinical and immunological features of severe and
820 moderate coronavirus disease 2019. *J Clin Invest* 2020;130(5):2620–9.
- 821 33. Knight DS, Kotecha T, Razvi Y, et al. COVID-19: Myocardial injury in
822 survivors. *Circulation*. 2020;
- 823 34. Del Valle DM, Kim-Schulze S, Huang HH, et al. An inflammatory cytokine
824 signature predicts COVID-19 severity and survival. *Nat Med* 2020;
- 825 35. Mehta P, McAuley DF, Brown M, Sanchez E, Tattersall RS, Manson JJ. COVID-
826 19: consider cytokine storm syndromes and immunosuppression. *Lancet*. 2020;
- 827 36. Polidoro RB, Hagan RS, de Santis Santiago R, Schmidt NW. Overview:
828 Systemic Inflammatory Response Derived From Lung Injury Caused by SARS-
829 CoV-2 Infection Explains Severe Outcomes in COVID-19. *Front. Immunol*.
830 2020;
- 831 37. Shen B, Yi X, Sun Y, et al. Proteomic and Metabolomic Characterization of
832 COVID-19 Patient Sera. *Cell* 2020;
- 833 38. Delafiori J, Claudio Navarro L, Focaccia Siciliano R, et al. Covid-19 automated
834 diagnosis and risk assessment through Metabolomics and Machine-Learning.
835 2020.
- 836 39. Bittleman DB, Casale TB. 5-Hydroxyeicosatetraenoic acid (HETE)-induced
837 neutrophil transcellular migration is dependent upon enantiomeric structure. *Am*
838 *J Respir Cell Mol Biol* 1995;12(3):260–7.
- 839 40. Harder DR. Pressure-induced myogenic activation of cat cerebral arteries is
840 dependent on intact endothelium. *Circ Res* 1987;
- 841 41. Barnes BJ, Adrover JM, Baxter-Stoltzfus A, et al. Targeting potential drivers of
842 COVID-19: Neutrophil extracellular traps. *J. Exp. Med.* 2020;

- 843 42. Kita Y, Takahashi T, Uozumi N, Nallan L, Gelb MH, Shimizu T. Pathway-
844 oriented profiling of lipid mediators in macrophages. *Biochem Biophys Res*
845 *Commun* 2005;
- 846 43. Gauthier KM, Goldman DH, Aggarwal NT, Chawengsub Y, Falck JR, Campbell
847 WB. Role of arachidonic acid lipoxygenase metabolites in acetylcholine-induced
848 relaxations of mouse arteries. *Am J Physiol - Hear Circ Physiol* 2011;
- 849 44. Rauzi F, Kirkby NS, Edin ML, et al. Aspirin inhibits the production of
850 proangiogenic 15(S)-HETE by platelet cyclooxygenase-1. *FASEB J* 2016;
- 851 45. Berna N, Arnould T, Remacle J, Michiels C. Hypoxia-induced increase in
852 intracellular calcium concentration in endothelial cells: Role of the Na⁺-glucose
853 cotransporter. *J Cell Biochem* 2002;
- 854 46. López S, Vila L, Breviario F, de Castellarnau C. Interleukin-1 increases 15-
855 hydroxyecosatetraenoic acid formation in cultured human endothelial cells.
856 *Biochim Biophys Acta (BBA)/Lipids Lipid Metab* 1993;
- 857 47. Metz SA, Murphy RC, Fujimoto W, . Effects on glucose-induced insulin
858 secretion of lipoxygenase-derived metabolites of arachidonic acid. *Diabetes*
859 1984;33(2):119–24.
- 860 48. Hosoi T, Koguchi Y, Sugikawa E, et al. Identification of a novel human
861 eicosanoid receptor coupled to Gi/o. *J Biol Chem* 2002;
- 862 49. Powell WS, Rokach J, . . The eosinophil chemoattractant 5-oxo-ETE and the
863 OXE receptor. *Prog. Lipid Res.* 2013;
- 864 50. Powell WS, Rokach J. Targeting the OXE receptor as a potential novel therapy
865 for asthma. *Biochem Pharmacol* 2020;179:113930.
- 866 51. Schwarz B, Sharma L, Roberts L, et al. Cutting Edge: Severe SARS-CoV-2
867 Infection in Humans Is Defined by a Shift in the Serum Lipidome, Resulting in

- 868 Dysregulation of Eicosanoid Immune Mediators. *J Immunol* [Internet]
869 2020;ji2001025. Available from:
870 <http://www.jimmunol.org/content/early/2020/12/04/jimmunol.2001025.abstract>
- 871 52. Hanna VS, Hafez EAA. Synopsis of arachidonic acid metabolism: A review. *J.*
872 *Adv. Res.* 2018;
- 873 53. Schwarz B, Sharma L, Roberts L, et al. Severe SARS-CoV-2 infection in humans
874 is defined by a shift in the serum lipidome resulting in dysregulation of
875 eicosanoid immune mediators. *Res Sq* 2020;
- 876 54. Nienhold R, Ciani Y, Koelzer VH, et al. Two distinct immunopathological
877 profiles in autopsy lungs of COVID-19. *Nat Commun* [Internet]
878 2020;11(1):5086. Available from: <https://doi.org/10.1038/s41467-020-18854-2>
- 879 55. Pairo-Castineira E, Clohisey S, Klaric L, et al. Genetic mechanisms of critical
880 illness in Covid-19. *Nature* [Internet] 2020; Available from:
881 <https://doi.org/10.1038/s41586-020-03065-y>
- 882 56. Taha AY. Linoleic acid—good or bad for the brain? *npj Sci. Food.* 2020;
- 883 57. Kohn A, Gitelman J, Inbar M. Unsaturated free fatty acids inactivate animal
884 enveloped viruses. *Arch Virol* 1980;
- 885 58. Das UN. Arachidonic acid and other unsaturated fatty acids and some of their
886 metabolites function as endogenous antimicrobial molecules: A review. *J. Adv.*
887 *Res.* 2018;
- 888 59. Chandrasekharan JA, Sharma-Walia N. Arachidonic acid derived lipid mediators
889 influence Kaposi's sarcoma-associated herpesvirus infection and pathogenesis.
890 *Front. Microbiol.* 2019;
- 891 60. Das UN. Bioactive Lipids in COVID-19-Further Evidence. *Arch Med Res* 2020;
- 892 61. Nakano T, Ohara O, Teraoka H, Arita H. Glucocorticoids suppress group II

- 893 phospholipase A2 production by blocking mRNA synthesis and post-
894 transcriptional expression. *J Biol Chem* 1990;
- 895 62. Kobza Black A, Greaves M, Hensby C. The effect of systemic prednisolone on
896 arachidonic acid, and prostaglandin E2 and F2 alpha levels in human cutaneous
897 inflammation. *Br J Clin Pharmacol* 1982;
- 898 63. Hu X, Cifarelli V, Sun S, Kuda O, Abumrad NA, Su X. Major role of adipocyte
899 prostaglandin E2 in lipolysis-induced macrophage recruitment. *J Lipid Res* 2016;
- 900 64. Alzoghaibi MA, Walsh SW, Willey A, Yager DR, Fowler AA, Graham MF.
901 Linoleic acid induces interleukin-8 production by Crohn's human intestinal
902 smooth muscle cells via arachidonic acid metabolites. *Am J Physiol -*
903 *Gastrointest Liver Physiol* 2004;
- 904 65. Ahn K, McKinney MK, Cravatt BF. Enzymatic pathways that regulate
905 endocannabinoid signaling in the nervous system. *Chem Rev* 2008;108(5):1687–
906 707.
- 907 66. Grant RA, Morales-Nebreda L, Markov NS, et al. Alveolitis in severe SARS-
908 CoV-2 pneumonia is driven by self-sustaining circuits between infected alveolar
909 macrophages and T cells. *bioRxiv* 2020;
- 910 67. Malcher-Lopes R, Franco A, Tasker JG. Glucocorticoids shift arachidonic acid
911 metabolism toward endocannabinoid synthesis: A non-genomic anti-
912 inflammatory switch. *Eur. J. Pharmacol.* 2008;
- 913 68. The RECOVERY Collaborative G. Dexamethasone in Hospitalized Patients with
914 Covid-19 — Preliminary Report. *N Engl J Med* 2020;
- 915 69. Tomazini BM, Maia IS, Cavalcanti AB, et al. Effect of Dexamethasone on Days
916 Alive and Ventilator-Free in Patients with Moderate or Severe Acute Respiratory
917 Distress Syndrome and COVID-19: The CoDEX Randomized Clinical Trial.

- 918 JAMA - J Am Med Assoc 2020;
- 919 70. Tang Y, Liu J, Zhang D, Xu Z, Ji J, Wen C. Cytokine Storm in COVID-19: The
920 Current Evidence and Treatment Strategies. *Front. Immunol.* 2020;
- 921 71. Ye Q, Wang B, Mao J, . The pathogenesis and treatment of the ‘Cytokine
922 Storm’’ in COVID-19.’ *J. Infect.* 2020;
- 923 72. Prescott HC, Rice TW. Corticosteroids in COVID-19 ARDS: Evidence and Hope
924 during the Pandemic. *JAMA - J. Am. Med. Assoc.* 2020;
- 925 73. Noushmehr H, D’Amico E, Farilla L, et al. Fatty acid translocase (FAT/CD36) is
926 localized on insulin-containing granules in human pancreatic β -cells and
927 mediates fatty acid effects on insulin secretion. *Diabetes* 2005;
- 928 74. Glatz JFC, Luiken J. From fat to FAT (CD36/SR-B2): Understanding the
929 regulation of cellular fatty acid uptake. *Biochimie.* 2017;
- 930 75. Febbraio M, Hajjar DP, Silverstein RL. CD36: A class B scavenger receptor
931 involved in angiogenesis, atherosclerosis, inflammation, and lipid metabolism. *J.*
932 *Clin. Invest.* 2001;
- 933 76. Glatz JFC, Luiken JJFP, Bonen A. Membrane fatty acid transporters as regulators
934 of lipid metabolism: Implications for metabolic disease. *Physiol. Rev.* 2010;
- 935 77. Pepino MY, Kuda O, Samovski D, Abumrad NA. Structure-function of CD36
936 and importance of fatty acid signal transduction in fat metabolism. *Annu. Rev.*
937 *Nutr.* 2014;
- 938 78. Zoccal KF, Gardinassi LG, Sorgi CA, et al. CD36 shunts eicosanoid metabolism
939 to repress CD14 Licensed interleukin-1 β release and inflammation. *Front*
940 *Immunol* 2018;
- 941 79. Khan NA, Besnard P. Oro-sensory perception of dietary lipids: New insights into
942 the fat taste transduction. *Biochim. Biophys. Acta - Mol. Cell Biol. Lipids.* 2009;

- 943 80. Deleon-Pennell KY, Tian Y, Zhang B, et al. CD36 Is a Matrix Metalloproteinase-
944 9 Substrate That Stimulates Neutrophil Apoptosis and Removal during Cardiac
945 Remodeling. *Circ Cardiovasc Genet* 2016;
- 946 81. Novak ML, Thorp EB. Shedding light on impaired efferocytosis and
947 nonresolving inflammation. *Circ. Res.* 2013;
- 948 82. Cundall M, Sun Y, Miranda C, Trudeau JB, Barnes S, Wenzel SE. Neutrophil-
949 derived matrix metalloproteinase-9 is increased in severe asthma and poorly
950 inhibited by glucocorticoids. *J Allergy Clin Immunol* 2003;
- 951 83. Hozumi A, Nishimura Y, Nishiuma T, Kotani Y, Yokoyama M. Induction of
952 MMP-9 in normal human bronchial epithelial cells by TNF- α via NF- κ B-
953 mediated pathway. *Am J Physiol - Lung Cell Mol Physiol* 2001;
- 954 84. Ueland T, Holter JC, Holten AR, et al. Distinct and early increase in circulating
955 MMP-9 in COVID-19 patients with respiratory failure: MMP-9 and respiratory
956 failure in COVID-19. *J. Infect.* 2020;
- 957 85. Palau V, Riera M, Soler MJ. ADAM17 inhibition may exert a protective effect
958 on COVID-19. *Nephrol Dial Transplant* 2020;
- 959 86. Laing AG, Lorenc A, del Molino del Barrio I, et al. A dynamic COVID-19
960 immune signature includes associations with poor prognosis. *Nat Med* 2020;
- 961 87. Zhao Y, Qin L, Zhang P, et al. Longitudinal COVID-19 profiling associates IL-
962 1RA and IL-10 with disease severity and RANTES with mild disease. *JCI Insight*
963 2020;
- 964 88. Belge K-U, Dayyani F, Horelt A, et al. The Proinflammatory CD14 + CD16 +
965 DR ++ Monocytes Are a Major Source of TNF . *J Immunol* 2002;
- 966 89. Kunkel SL, Standiford T, Kasahara K, Strieter RM. Interleukin-8 (IL-8): The
967 major neutrophil chemotactic factor in the lung. *Exp Lung Res* 1991;

- 968 90. Kunkel TA, Bebenek K, McClary J. Efficient site-directed mutagenesis using
969 uracil-containing DNA. *Methods Enzymol* 1991;
- 970 91. Zoccal KF, Sorgi CA, Hori JI, et al. Opposing roles of LTB4 and PGE2 in
971 regulating the inflammasome-dependent scorpion venom-induced mortality. *Nat*
972 *Commun* 2016;
- 973 92. De Virgiliis F, Di Giovanni S. Lung innervation in the eye of a cytokine storm:
974 neuroimmune interactions and COVID-19. *Nat Rev Neurol* 2020;
- 975 93. Carmona-Rivera C, Purmalek MM, Moore E, et al. A role for muscarinic
976 receptors in neutrophil extracellular trap formation and levamisole-induced
977 autoimmunity. *JCI Insight* 2017;
- 978 94. do Espírito Santo DA, Lemos ACB, Miranda CH, . In vivo demonstration of
979 microvascular thrombosis in severe COVID-19. *J Thromb Thrombolysis* 2020;
- 980 95. Supuran CT, Di Fiore A, De Simone G. Carbonic anhydrase inhibitors as
981 emerging drugs for the treatment of obesity. *Expert Opin. Emerg. Drugs.* 2008;
- 982 96. Cavallotti C, Bruzzone P, Mancone M, Leali FMT. Distribution of
983 acetylcholinesterase and cholineacetyl-transferase activities in coronary vessels
984 of younger and older adults. *Geriatr Gerontol Int* 2004;
- 985 97. Vijayaraghavan S, Huang B, Blumenthal EM, Berg DK. Arachidonic acid as a
986 possible negative feedback inhibitor of nicotinic acetylcholine receptors on
987 neurons. *J Neurosci* 1995;
- 988 98. Mabley J, Gordon S, Pacher P. Nicotine exerts an anti-inflammatory effect in a
989 murine model of acute lung injury. *Inflammation* 2011;
- 990 99. Blanco-Melo D, Nilsson-Payant BE, Liu WC, et al. Imbalanced Host Response to
991 SARS-CoV-2 Drives Development of COVID-19. *Cell* 2020;
- 992 100. Horiguchi K, Horiguchi S, Yamashita N, et al. Expression of SLURP-1, an

- 993 endogenous $\alpha 7$ nicotinic acetylcholine receptor allosteric ligand, in murine
994 bronchial epithelial cells. *J Neurosci Res* 2009;
- 995 101. Schirmer SU, Eckhardt I, Lau H, et al. The cholinergic system in rat testis is of
996 non-neuronal origin. *Reproduction* 2011;
- 997 102. Suenaga A, Fujii T, Ogawa H, et al. Up-regulation of lymphocytic cholinergic
998 activity by ONO-4819, a selective prostaglandin EP4 receptor agonist, in MOLT-
999 3 human leukemic T cells. *Vascul Pharmacol* 2004;
- 1000 103. Reinheimer T, Münch M, Bittinger F, Racké K, Kirkpatrick CJ, Wessler I.
1001 Glucocorticoids mediate reduction of epithelial acetylcholine content in the
1002 airways of rats and humans. *Eur J Pharmacol* 1998;
- 1003 104. Gross I, Ballard PL, Ballard RA, Jones CT, Wilson CM. Corticosteroid
1004 stimulation of phosphatidylcholine synthesis in cultured fetal rabbit lung:
1005 Evidence for de novo protein synthesis mediated by glucocorticoid receptors.
1006 *Endocrinology* 1983;
- 1007 105. Nakamura T, Fujiwara R, Ishiguro N, et al. Involvement of choline transporter-
1008 like proteins, CTL1 and CTL2, in glucocorticoid-induced acceleration of
1009 phosphatidylcholine synthesis via increased choline uptake. *Biol Pharm Bull*
1010 2010;
- 1011 106. Wilk JB, Shrine NRG, Loehr LR, et al. Genome-wide association studies identify
1012 *CHRNA5/3* and *HTR4* in the development of airflow obstruction. *Am J Respir*
1013 *Crit Care Med* 2012;
- 1014 107. Lam DCL, Luo SY, Fu KH, et al. Nicotinic acetylcholine receptor expression in
1015 human airway correlates with lung function. *Am J Physiol - Lung Cell Mol*
1016 *Physiol* 2016;
- 1017 108. Oenema TA, Kolahian S, Nanninga JE, et al. Pro-inflammatory mechanisms of

- 1018 muscarinic receptor stimulation in airway smooth muscle. *Respir Res* 2010;
- 1019 109. Yamada M, Ichinose M. The cholinergic pathways in inflammation: A potential
1020 pharmacotherapeutic target for COPD. *Front. Pharmacol.* 2018;
- 1021 110. Fadason T, Schierding W, Lumley T, O'Sullivan JM. Chromatin interactions and
1022 expression quantitative trait loci reveal genetic drivers of multimorbidities. *Nat*
1023 *Commun* 2018;9(1):5198.
- 1024 111. Lagoumintzis G, Chasapis CT, Alexandris N, et al. COVID-19 and Cholinergic
1025 Anti-inflammatory Pathway: *In silico* Identification of an
1026 Interaction between $\alpha 7$ Nicotinic Acetylcholine Receptor and the Cryptic
1027 Epitopes of SARS-CoV and SARS-CoV-2 Spike Glycoproteins. *bioRxiv*
1028 [Internet] 2020;2020.08.20.259747. Available from:
1029 <http://biorxiv.org/content/early/2020/08/21/2020.08.20.259747.abstract>
- 1030 112. Gahring LC, Myers EJ, Dunn DM, Weiss RB, Rogers SW. Nicotinic alpha 7
1031 receptor expression and modulation of the lung epithelial response to
1032 lipopolysaccharide. *PLoS One* 2017;
- 1033 113. Wang H, Yu M, Ochani M, et al. Nicotinic acetylcholine receptor $\alpha 7$ subunit is
1034 an essential regulator of inflammation. *Nature* 2003;421(6921):384–8.
- 1035 114. Pinheiro NM, Santana FPR, Almeida RR, et al. Acute lung injury is reduced by
1036 the $\alpha 7$ nAChR agonist PNU-282987 through changes in the macrophage profile.
1037 *FASEB J* 2017;
- 1038 115. Hamano R, Takahashi HK, Iwagaki H, Yoshino T, Nishibori M, Tanaka N.
1039 Stimulation of $\alpha 7$ nicotinic acetylcholine receptor inhibits CD14 and the toll-like
1040 receptor 4 expression in human monocytes. *Shock* 2006;
- 1041 116. Hasday JD, Dubin W, Mongovin S, et al. Bronchoalveolar macrophage CD14
1042 expression: Shift between membrane- associated and soluble pools. *Am J Physiol*

- 1043 - Lung Cell Mol Physiol 1997;
- 1044 117. Gori S, Alcaín J, Vanzulli S, et al. Acetylcholine-treated murine dendritic cells
1045 promote inflammatory lung injury. PLoS One 2019;
- 1046 118. Edwards JM, McCarthy CG, Wenceslau CF. The Obligatory Role of the
1047 Acetylcholine-Induced Endothelium-Dependent Contraction in Hypertension:
1048 Can Arachidonic Acid Resolve this Inflammation? Curr Pharm Des 2020;
- 1049 119. Radu BM, Osculati AMM, Suku E, et al. All muscarinic acetylcholine receptors
1050 (M1-M5) are expressed in murine brain microvascular endothelium. Sci Rep
1051 2017;
- 1052 120. Kumar PT, Antony S, Nandhu MS, Sadanandan J, Naijil G, Paulose CS. Vitamin
1053 D3 restores altered cholinergic and insulin receptor expression in the cerebral
1054 cortex and muscarinic M3 receptor expression in pancreatic islets of
1055 streptozotocin induced diabetic rats. J Nutr Biochem 2011;
- 1056 121. Ali N. Role of vitamin D in preventing of COVID-19 infection, progression and
1057 severity. J. Infect. Public Health. 2020;
- 1058 122. CHANGEUX jean-pierre, Amoura Z, Rey F, Miyara M. A nicotinic hypothesis
1059 for Covid-19 with preventive and therapeutic implications. Qeios 2020;
- 1060 123. Oakes JM, Fuchs RM, Gardner JD, Lazartigues E, Yue X. Nicotine and the
1061 renin-angiotensin system. Am. J. Physiol. - Regul. Integr. Comp. Physiol. 2018;
- 1062 124. Nct. Pyridostigmine in Severe SARS-CoV-2 Infection.
1063 <https://clinicaltrials.gov/show/NCT04343963> 2020;
- 1064 125. Ahmed H O. COVID-19: Targeting the cytokine storm via cholinergic anti-
1065 inflammatory (Pyridostigmine). Int J Clin Virol 2020;
- 1066 126. Gonzalez-Rubio J, Navarro-Lopez C, Lopez-Najera E, et al. Cytokine Release
1067 Syndrome (CRS) and Nicotine in COVID-19 Patients: Trying to Calm the Storm.

- 1068 Front Immunol 2020;
- 1069 127. ahir AMOURA FT. Efficacy of Nicotine in Preventing COVID-19 Infection in
1070 Caregivers (NICOVID-PREV). Natl Libr Med 2020;2:1–8.
- 1071 128. Smith JC, Sausville EL, Girish V, et al. Cigarette Smoke Exposure and
1072 Inflammatory Signaling Increase the Expression of the SARS-CoV-2 Receptor
1073 ACE2 in the Respiratory Tract. Dev Cell 2020;
- 1074 129. Leung JM, Leung JM, Yang CX, Sin DD, Sin DD. COVID-19 and nicotine as a
1075 mediator of ACE-2. Eur. Respir. J. 2020;
- 1076 130. Zureik M, Baricault B, Vabre C, et al. Nicotine-replacement therapy as a
1077 surrogate of smoking and the risk of hospitalization with Covid-19 and all-cause
1078 mortality a nationwide observational cohort study in France. medrxiv 2020;
- 1079 131. Margină D, Ungurianu A, Purdel C, et al. Chronic inflammation in the context of
1080 everyday life: Dietary changes as mitigating factors. Int. J. Environ. Res. Public
1081 Health. 2020;
- 1082 132. Hadjadj J, Yatim N, Barnabei L, et al. Impaired type I interferon activity and
1083 inflammatory responses in severe COVID-19 patients. Science (80-) 2020;
- 1084 133. Ye G, Pan Z, Pan Y, et al. Clinical characteristics of severe acute respiratory
1085 syndrome coronavirus 2 reactivation. J Infect 2020;
- 1086 134. Xu XW, Wu XX, Jiang XG, et al. Clinical findings in a group of patients infected
1087 with the 2019 novel coronavirus (SARS-Cov-2) outside of Wuhan, China:
1088 Retrospective case series. BMJ 2020;
- 1089 135. Grasselli G, Zangrillo A, Zanella A, et al. Baseline Characteristics and Outcomes
1090 of 1591 Patients Infected with SARS-CoV-2 Admitted to ICUs of the Lombardy
1091 Region, Italy. JAMA - J Am Med Assoc 2020;
- 1092 136. Marshall JC, Murthy S, Diaz J, et al. A minimal common outcome measure set

- 1093 for COVID-19 clinical research. *Lancet Infect. Dis.* 2020;
- 1094 137. Office WHOEMR. Updated clinical management guideline for COVID-19.
1095 *Wkly. Epidemiol. Monit.* 2020;
- 1096 138. Rauch A, Labreuche J, Lassalle F, et al. Coagulation biomarkers are independent
1097 predictors of increased oxygen requirements in COVID-19. *J Thromb Haemost*
1098 2020;
- 1099 139. Sahu BR, Kampa RK, Padhi A, Panda AK. C-reactive protein: A promising
1100 biomarker for poor prognosis in COVID-19 infection. *Clin Chim Acta* 2020;
- 1101 140. Richardson S, Hirsch JS, Narasimhan M, et al. Presenting Characteristics,
1102 Comorbidities, and Outcomes Among 5700 Patients Hospitalized With COVID-
1103 19 in the New York City Area. *JAMA [Internet]* 2020;323(20):2052–9. Available
1104 from: <https://doi.org/10.1001/jama.2020.6775>
- 1105 141. Thomas T, Stefanoni D, Reisz J, et al. COVID-19 infection results in alterations
1106 of the kynurenine pathway and fatty acid metabolism that correlate with IL-6
1107 levels and renal status. *medRxiv Prepr Serv Heal Sci* 2020;
- 1108 142. Moolamalla STR, Chauhan R, Priyakumar D, Vinod PK. Host metabolic
1109 reprogramming in response to SARS-Cov-2 infection. *bioRxiv* 2020;
- 1110 143. Soliman S, Faris MAIE, Ratemi Z, Halwani R. Switching Host Metabolism as an
1111 Approach to Dampen SARS-CoV-2 Infection. *Ann. Nutr. Metab.* 2020;
- 1112 144. Frankenberger M, Sternsdorf T, Pechumer H, Pforte A, Ziegler-Heitbrock HWL.
1113 Differential cytokine expression in human blood monocyte subpopulations: A
1114 polymerase chain reaction analysis. *Blood* 1996;
- 1115 145. Giamarellos-Bourboulis EJ, Netea MG, Rovina N, et al. Complex Immune
1116 Dysregulation in COVID-19 Patients with Severe Respiratory Failure. *Cell Host*
1117 *Microbe* 2020;

1118 146. Lamontagne F, Brower R, Meade M. Corticosteroid therapy in acute respiratory
1119 distress syndrome. *CMAJ*. 2013;

1120 147. Russell CD, Millar JE, Baillie JK. Clinical evidence does not support
1121 corticosteroid treatment for 2019-nCoV lung injury. *Lancet*. 2020;

1122

1123 **Acknowledgements**

1124 The authors thankfully acknowledge Innovation and Technology Park (Supera), the
1125 healthy-participants joining as controls and the positive COVID-19 patients as well as
1126 their families. We grieve for all patients who lost their lives as a result of this pandemic,
1127 including those who provided us with samples to be able to answer scientific questions
1128 and contribute to humanity's eradication of this disease. We also thank Fabiana Rossetto
1129 de Moraes, B.Sc., for the cytometry analysis, Caroline Fontanari, M.Sc., for laboratory
1130 and technical support, the ICU team, and all hospital professionals, especially the
1131 technicians, nurses, physiotherapists, and biomedical personnel, who collaborated on this
1132 work through Hospital Santa Casa de Misericórdia in Ribeirão Preto and Hospital São
1133 Paulo in Ribeirão Preto. We are grateful for the indispensable contribution of the Ribeirão
1134 Preto Municipal Health Department and the employees of the Serviço de Análises
1135 Clínicas (SAC) of the Faculdade de Ciências Farmacêuticas de Ribeirão Preto, USP. We
1136 also thank Professors Victor Hugo Aquino Quintana, Ph.D., Márcia Regina von Zeska
1137 Kress, Ph.D., and Marcia Eliana da Silva Ferreira, Ph.D. for sharing the BSL2 viral
1138 laboratory.

1139

1140

1141 **Additional Information**

1142 Extended data available in Supplementary Appendixes:

1143 • Supplementary Appendix I - Pathways and list of corresponding genes related to
1144 acetylcholine and arachidonic acid observed in Reactome pathways and Covid-19
1145 biomarkers.

1146

1147 • Supplementary Appendix II - Report of CEMITool results for the gene co-
1148 expression modular analysis of lung samples from biopsies of Covid-19 and non-
1149 Covid-19 patients.

1150

1151 • Supplementary Appendix III - Differential gene expression analysis results
1152 between Covid-19-death groups (CV, NCV, CVL and CVH) and Covid-19
1153 samples from patients who underwent glucocorticoid treatment (GC) and not
1154 (non-GC).

1155

1156 • Supplementary Appendix IV - Betweenness and degree values of genes from
1157 biological network constructed based on the principal co-expression module M1.

1158

1159

1160 **Funding**

1161 Fundação de Amparo a Pesquisa do Estado de São Paulo (FAPESP):
1162 #2020/05207-6, #2014/07125-6 and #2015/00658-1 for **L.H.F.**; #2020/08534-8 for
1163 **M.M.P.**; #2018/22667-0 for **C.O.S.S.**; #2020/05270-0 for **V.D.B.** Additional support was

1164 provided by the National Council for Scientific and Technological Development (CNPq),
1165 the Coordination for the Improvement of Higher Educational Personnel (CAPES-Finance
1166 Code 001)), and Pró-Reitora de Pesquisa da Universidade de São Paulo, grant-USP-
1167 VIDA.

1168 **Conflict of Interest Statement**

1169 The authors declare that this research was performed without conflicts of interest
1170 or commercial or financial gains.

1171 **Legends of main figures**

1172 **Figure 1. Metabolomic and lipidomic analysis revealed increased levels of**
1173 **circulating fatty acids, arachidonic acid (AA), 5-HETE and 11-HETE in patients**
1174 **with Covid-19.**

1175 Plasma samples were collected from healthy-participants (n=20) and patients with
1176 asymptomatic-to-mild (n=10), moderate (n=12), severe (n=16), or critical (n=13) disease.
1177 (A) A Manhattan plot for the differential abundance of metabolite features in different
1178 groups of patients with Covid-19 and healthy participants (false discovery rate (FDR) of
1179 595, adjusted $P < 0.05$, above the dashed line) and (B, left panel) metabolic pathway
1180 enrichment of significant metabolite features based on data from untargeted mass
1181 spectrometry. Differential abundance was calculated using the *limma* package for R, and
1182 FDR was controlled using the Benjamini-Hochberg method. Mummichog software v2.3.3
1183 was used for pathway enrichment analysis. (B, right panel) Schematic illustration of the
1184 metabolic pathways involved in the production of hydroxyeicosatetraenoic acids
1185 (HETEs), such as 5-HETE and 11-HETE, from arachidonic (AA) and linoleic acid
1186 metabolism, which discriminate the severity of Covid-19. (C-E) Plasma metabolomics

1187 indicating an increase in free fatty acids in Covid-19. Plasma obtained from healthy
1188 participants (n=18) and patients with asymptomatic-to-mild (n=10), moderate (n=12),
1189 severe (n=14), or critical (n=16) disease (F-H) was subjected to lipidomics analysis using
1190 targeted mass spectrometry, confirming the elevation of AA, 5-HETE and 11-HETE,
1191 according to the severity of Covid-19. Data are expressed as the mean \pm SEM. Differences
1192 in (C-H) were considered significant at $P < 0.05$ according to Kruskal–Wallis analysis
1193 followed by Dunn’s posttest, and specific P-values are shown in each figure.

1194

1195 **Figure 2. Systemic markers of inflammation determined Covid-19 severity.**

1196 (A-F) Total and differential leukocyte counts in peripheral blood from healthy-
1197 participants (n=17) and from patients with asymptomatic-to-mild (n=10), moderate
1198 (n=12), severe (n=16) or critical (n=13) disease showed that Covid-19 modified the
1199 numbers of distinct leukocyte populations. (G-H) Flow cytometry analysis of
1200 CD14⁺HLA-DR circulating monocytes by t-distributed stochastic neighbour embedding
1201 indicated reduced (G) CD14 and (H) CD36 mean fluorescence intensity in asymptomatic-
1202 to-mild (n=16), moderate (n=15), severe (n=35), and critical (n=20) Covid-19 patients
1203 compared to healthy participants (n=12). (I) Soluble CD14 (sCD14), as determined by
1204 ELISA) in healthy participants (n=12), asymptomatic-to-mild (n=12), moderate (n=13),
1205 severe (n=15), and critical (n=15) patients, showed increases only in samples from critical
1206 Covid-19 patients. (J-L) Classical, intermediate, and nonclassical monocytes determined
1207 by flow cytometry analyses of CD14, CD16 and HLA-DR expression in blood cells from
1208 healthy participants (n=12), asymptomatic-to-mild (n=16), moderate (n=15), severe
1209 (n=35), and critical (n=20) Covid-19 patients revealed a decrease in intermediate
1210 monocytes in Covid-19. (M-Q) Cytokines (IL-8, IL-6, IL-1 β , TNF and IL-10) quantified

1211 in plasma using a Cytometric Bead Array (CBA) of healthy volunteers (n=35),
1212 asymptomatic-to-mild (n=29), moderate (n=35), severe (n=42), and critical (n=21)
1213 patients demonstrated a distinct cytokine profile according to disease severity. Data are
1214 expressed as the mean \pm SEM, and differences between groups were calculated using
1215 Kruskal–Wallis with Dunn’s multiple comparison post-tests. The specific P-values are
1216 displayed in each figure. Differences were considered significant at $P < 0.05$.

1217

1218 **Figure 3. Altered production of lipid mediators and cellular infiltrates in the lungs**
1219 **drove the local response to SARS-CoV-2 infection.**

1220 BAL was collected from intubated patients with severe/critical confirmed Covid-
1221 19 diagnosis and from intubated patients without SARS-CoV-2 infection, which are
1222 labelled as Covid-19 and non-Covid-19, respectively. Data from untargeted mass
1223 spectrometry demonstrated (A) differential abundance of metabolite features comparing
1224 Covid-19 and non-Covid-19 participants (Manhattan plot, 595 at FDR adjusted $P < 0.05$,
1225 above the dashed line) and (B) metabolic pathway enrichment of significant metabolite
1226 features. Differential abundance was calculated using the *limma* package for R, and the
1227 false discovery rate was controlled using the Benjamini-Hochberg method; Covid-19
1228 (n=26) and non-Covid-19 (n=12). Mummichog software v2.3.3 was used for lipid
1229 pathway enrichment analysis. (C) Lipid mediators derived from arachidonic acid (AA)
1230 metabolism by lipoxygenase (LOX) or cyclooxygenase (COX) in both Covid-19 (n=19)
1231 and non-Covid-19 (n=11) samples, as determined by target mass spectrometry, showed a
1232 significant increase in 5-HETE and 11-HETE in Covid-19. (D) Total leukocytes in BAL
1233 fluid (left panel) and a representative image of Romanowsky staining in these cells (right
1234 panel) used for (E) identification of specific cellular populations in Covid-19 (n=23) and

1235 non-Covid-19 (n=11) patients showed a similar profile of infiltrating cells. (F) Cytokine
1236 concentrations in BAL from intubated Covid-19 patients (n=23) and non-Covid-19
1237 participants (n=11) also revealed a similar profile. (G, H) Classical and intermediate
1238 monocytes determined by flow cytometry analyses of CD14, CD16 and HLA-DR
1239 expression in BAL cells from Covid-19 (n=10) and non-Covid-19 (n=11) patients
1240 demonstrate that both populations are decreased in Covid-19. (I) CD14 and (J) CD36
1241 mean fluorescence intensity (MFI) of CD14⁺HLA-DR gated BAL monocytes is
1242 decreased in Covid-19 (n=10) compared to non-Covid-19 (n=11) patients. 5-HPETE: 5-
1243 hydroperoxyeicosatetraenoic acid, LTA₄: leukotriene A₄, LTA₄ hydrolase: leukotriene A₄
1244 hydrolase, LTB₄: leukotriene B₄, 6-trans LTB₄: 6-trans leukotriene B₄, 5-HETE: 5-
1245 hydroxyeicosatetraenoic acid, 11-HETE: 11-hydroxyeicosatetraenoic acid, 12-HETE:
1246 12-hydroxyeicosatetraenoic acid, 15-HETE: 15-hydroxyeicosatetraenoic acid, 5-oxo-
1247 HETE: 5-oxoeicosatetraenoic acid, 12-oxo-EETE: 12-oxoeicosatetraenoic acid, 15-oxo-
1248 HETE: 15-oxoeicosatetraenoic acid, PGH₂: prostaglandin H₂, PGE₂: prostaglandin E₂,
1249 PGD₂: prostaglandin D₂, TXB₂: thromboxane B, TX synthase: thromboxane. Data are
1250 expressed as the mean ± SEM. Differences between groups were calculated using the
1251 Mann–Whitney test, and specific P-values are shown in the figure. Differences were
1252 considered significant at P<0.05.

1253

1254 **Figure 4. Severe and critical phases of Covid-19 correlated with increased systemic**
1255 **and lung acetylcholine and lipid mediators, but only ACh was diminished by**
1256 **glucocorticoids**

1257 Comparison of systemic and local lung responses was analysed using blood and
1258 BAL samples from patients with severe/critical Covid-19 and showed that among (A)

1259 cytokines (plasma n=9; BAL n=9), (B) AA (plasma n=29; BAL n=19), (C) 5-HETE
1260 (plasma n=29; BAL n=19), and (D) 11-HETE (plasma n=29; BAL n=19), levels of only
1261 AA were higher in blood. (E) The ACh concentration (pmol.mL^{-1}) in heparinized plasma
1262 from healthy-participants (n=6) compared to plasma from SARS-CoV-2-infected patients
1263 not treated with glucocorticoids (non-GC) classified as having asymptomatic-to-mild
1264 (n=5), moderate (n=9), severe (n=7), and critical (n=7) disease showed an increase based
1265 on disease severity. (F) ACh in the plasma of patients with Covid-19 at severe/critical
1266 stages of the disease and treated (GC, n=18) or not (non-GC, n=14) with glucocorticoids
1267 shows decreased release in response to the treatment. (G) Comparison of ACh in BAL
1268 from SARS-CoV-2-infected severe/critical patients treated (CG, n=17) or not (non-GC,
1269 n=3) with glucocorticoids confirmed inhibition of the neurotransmitter by the treatment.
1270 (H) Comparison of neutrophil numbers from blood (n=14) and BAL (n=14) of patients
1271 with severe/critical disease demonstrated increased neutrophil infiltration in the lungs.
1272 Data are expressed as the mean \pm SEM. Differences were considered significant at $P < 0.05$
1273 according to (A) and (E) Kruskal–Wallis tests followed by Dunn’s posttest. (B, C, D, F
1274 and G) Student’s *t*-tests, Mann–Whitney, (H) Wilcoxon matched-pairs signed rank test.
1275 Concentrations of ACh in the blood of patients with severe and critical disease and not
1276 treated with glucocorticoids were the same, as shown in panels (E) and (F). Blood and
1277 BAL were collected during hospitalization, on average 6 to 17 days after admission, and
1278 glucocorticoids (methylprednisolone; range 40 to 500 mg/kg/day, or dexamethasone;
1279 range 1.5 to 6.0 mg/kg/day) were administered intravenously. Interaction networks
1280 between various pairs of mediators quantified in (I) blood (n=151) or (J) BAL (n=32)
1281 from our Covid-19 cohort, as constructed using the open access software Cytoscape v3.3
1282 (Cytoscape Consortium, San Diego, CA) and Spearman tests and showing significant
1283 correlations depicted by different lines (*r* and *P* values described in section 7.1). (K-P)

1284 Venn diagram constructed according to the online tool Draw Venn Diagram
1285 (<http://bioinformatics.psb.ugent.be/webtools/Venn/>) illustrates high-producing patients
1286 in severe and critical stages of disease, with (GC) or without (non-GC) treatment. (K-N)
1287 Plasma from patients producing high levels of AA, 5-HETE, 11-HETE, ACh and sCD14
1288 in GC (n=49) or non-GC (n=17) groups. (O, P) BAL from patients producing high levels
1289 of AA, 5-HETE, 11-HETE, and ACh in GC (n=23) or non-GC (n=4) groups. For analysis,
1290 the global median between controls and patients was considered as the cut-off point. (Q)
1291 Summary data of the values used for construction of the Venn diagrams. The table shows
1292 the absolute number of patients present at each stage of the disease and whether
1293 glucocorticoids were used for each molecule analysed. The percentage of individuals
1294 present in each experimental condition is highlighted in brackets.

1295

1296 **Figure 5. Re-analysis of transcriptome data reinforced the correlation between**
1297 **acetylcholine and arachidonic acid to Covid-19 severity and mortality.**

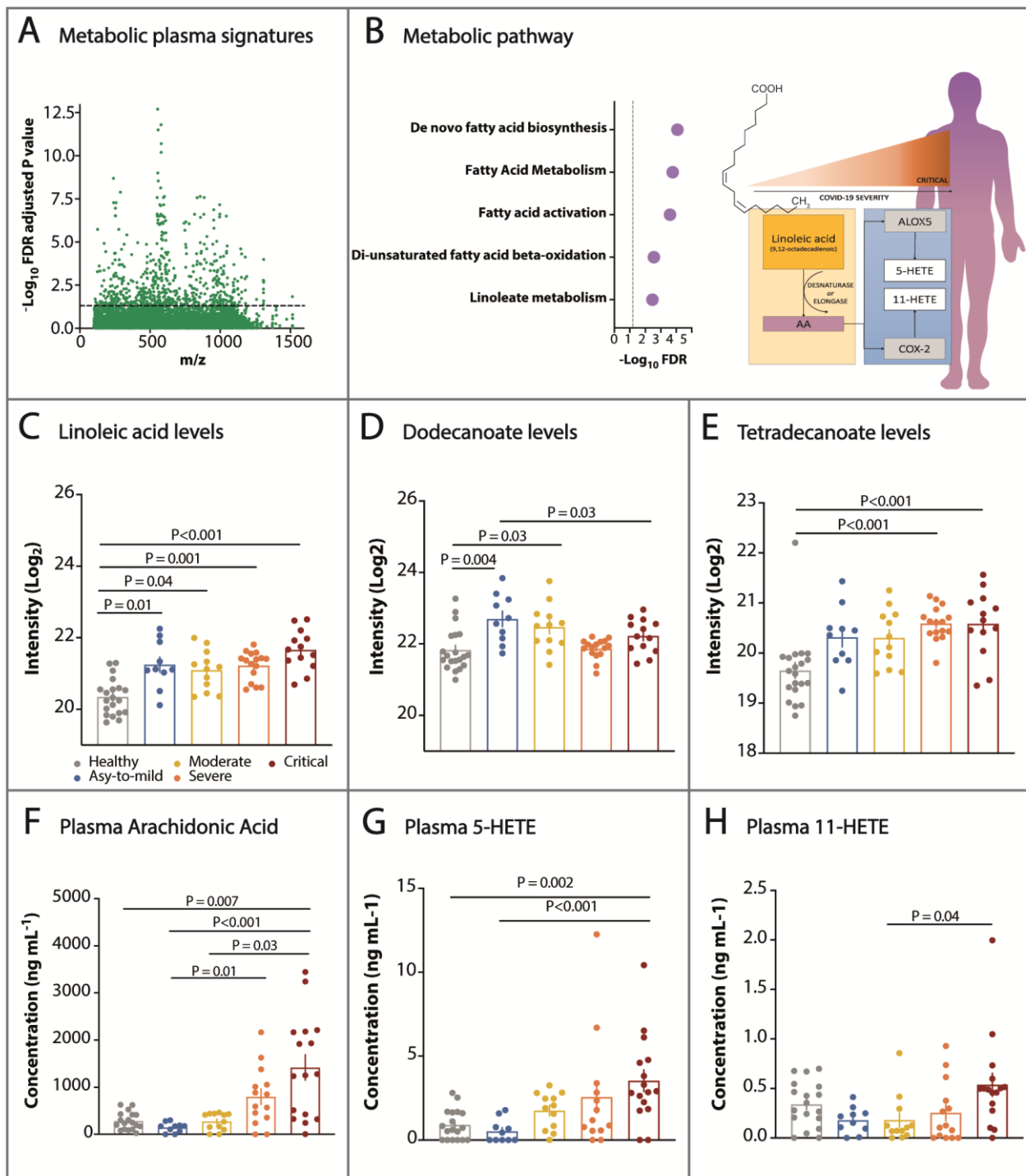
1298 (A) Gene coexpression profile from CVL, CVH, and NCV samples in principal
1299 module M1 (1047 genes, red lines) and mean gene expression (black line) (n=51). Genes
1300 identified as being associated with AA and ACh were only found in module M1; ten are
1301 related to cholinergic receptors and the ACh release cycle and eight to AA metabolism
1302 along with several biomarkers related to Covid-19 severity (Supplementary Appendix II;
1303 Table S4). (B) Heatmap of normalized gene expression related to the ACh and AA
1304 pathways and Covid-19 biomarkers (n=51). Almost all coexpressed genes of the ACh and
1305 AA pathways were upregulated in the CVL versus CVH group, including twelve
1306 cholinergic receptors, six ACh release cycle genes, eighteen AA production and
1307 metabolism pathway genes, and nine eicosanoid receptors (Figure S6A; Supplementary

1308 Appendix III). Approximately 36% of these genes were also upregulated in the CVL
1309 versus NCV group but not in the CV versus NCV group (n=51); among them, elongation
1310 of very long-chain fatty acid protein 2 (ELOVL2) is involved in linoleic acid metabolism
1311 (Figure S6A; Supplementary Appendix III). Cases 3, 9, and 11 were glucocorticoid-
1312 treated patients. (C) First-order gene interaction network of the M1 module containing
1313 differentially expressed genes related to ACh (brown), AA (green), Covid-19 biomarkers
1314 (red), betweenness hubs (blue), and albumin genes (magenta – Covid-19 biomarker and
1315 hub). Ten DEGs related to ACh and ten DEGs of AA populated the biological network
1316 and are connected to thirteen genes involved in the pathophysiology of Covid-19 and
1317 CD36. ACh- and AA-related genes showed relatively low values of centrality metrics and
1318 may be under the action of some hub genes, such as oestrogen receptor II (ESR2), insulin-
1319 like growth factor II mRNA binding protein (IGF2BP1), albumin (ALB), and others
1320 (Supplementary Appendix IV). (D) Plasma and BAL levels of ACh (n=52). ACh levels
1321 in BAL fluid exhibited a tendency towards increase compared to plasma samples from
1322 deceased or discharged patients. (E) AA (n= 48) and AA concentrations were higher in
1323 plasma than in BAL in both patient groups. (F) 5-HETE (n= 48) and (G) 11-HETE (n=47)
1324 in several/critical patients according to outcome (discharged or deceased). 5-HETE and
1325 11-HETE levels were only significantly higher in the BAL of deceased patients. (H)
1326 Transcription levels of cholinergic muscarinic M3 receptor (CHRM3) and cholinergic
1327 receptor nicotinic alpha 7 (CHRNA7) (n=51) and (I) oxoeicosanoid receptor 1 (OXER1)
1328 (n=51). A unique gene expression profile in lung samples from Covid-19 patients who
1329 had died was characterized by high levels of pro-inflammatory cholinergic receptors
1330 (CHRM3, CHRNA3, and CHRNA5)^{9,110}, low levels of anti-inflammatory cholinergic
1331 receptor (CHRNA7)¹¹³, and high expression of oxoeicosanoid receptor 1 (OXER1)⁵⁰
1332 which mediates the pro-inflammatory effects of eicosanoids (Figures S6B, S6C). Other

1333 eicosanoid and cholinergic receptors were also differentially expressed in CVL patients
1334 compared to the CVH or NCV group (Figures S6A, S6B, S6C). Finally, transcriptome
1335 analysis of fifteen Covid-19 and five non-Covid-19 samples indicated a correlation
1336 between ACh and AA genes and Covid-19 severity in some CVL patients. Significant
1337 differences in BAL/plasma levels of mediators were set at $P < 0.05$ according to the
1338 Kruskal-Wallis test followed by Dunn's posttest. *present in module M1. Abbreviations:
1339 Covid-19 low viral load (CVL) - Covid-19 high viral load (CVH) - non-Covid-19 (NCV).

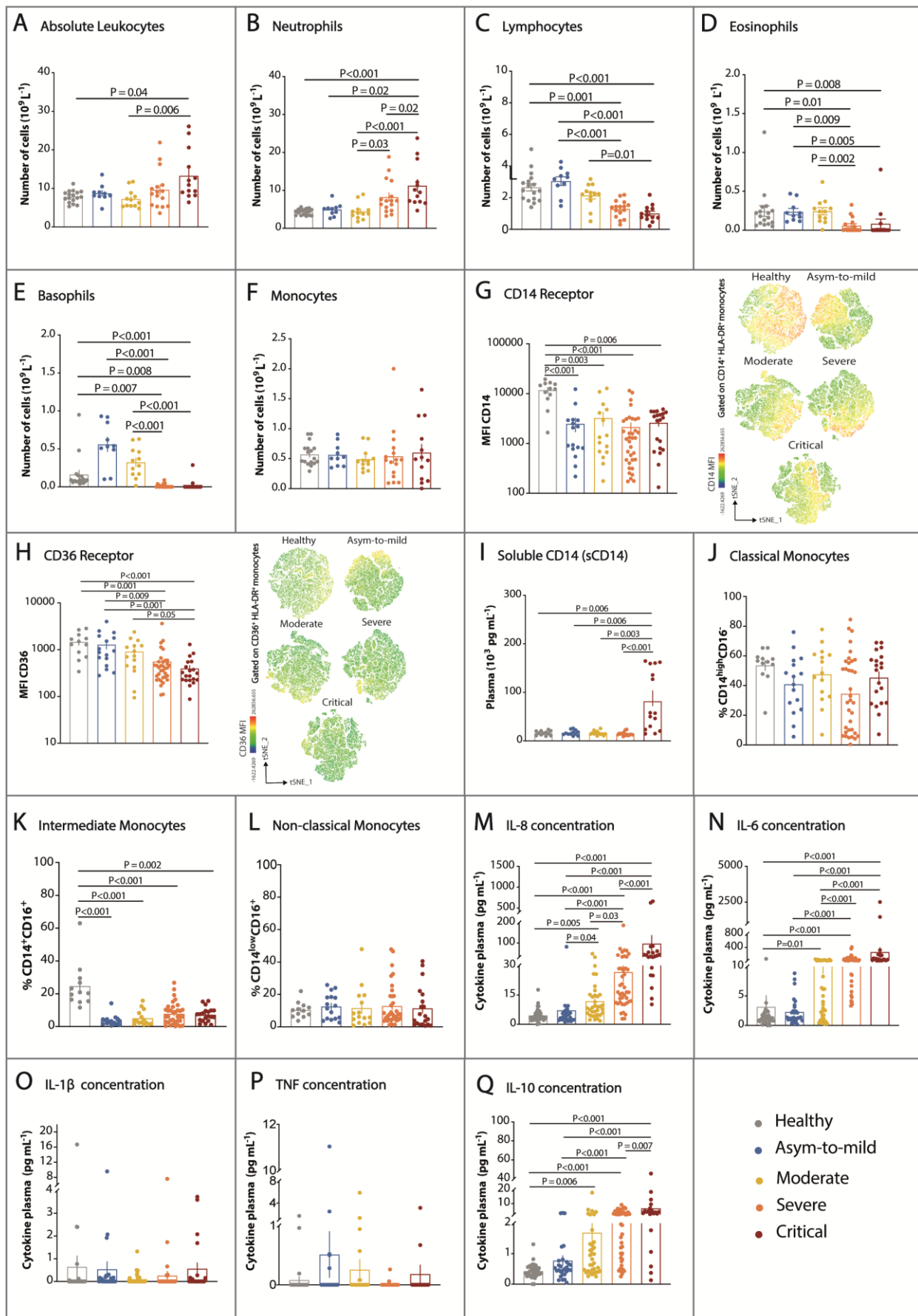
1340

Figure 1



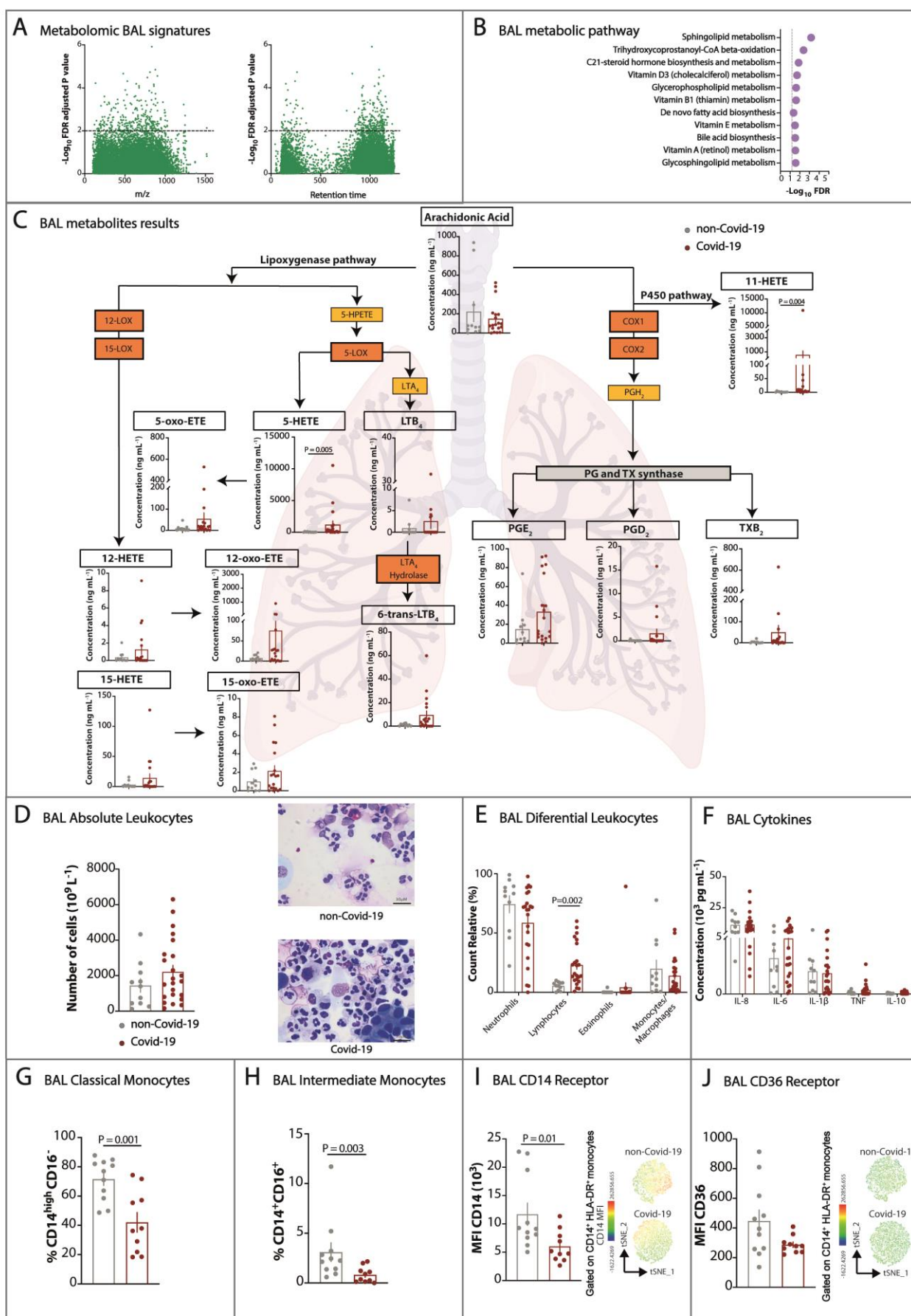
1341

Figure 2



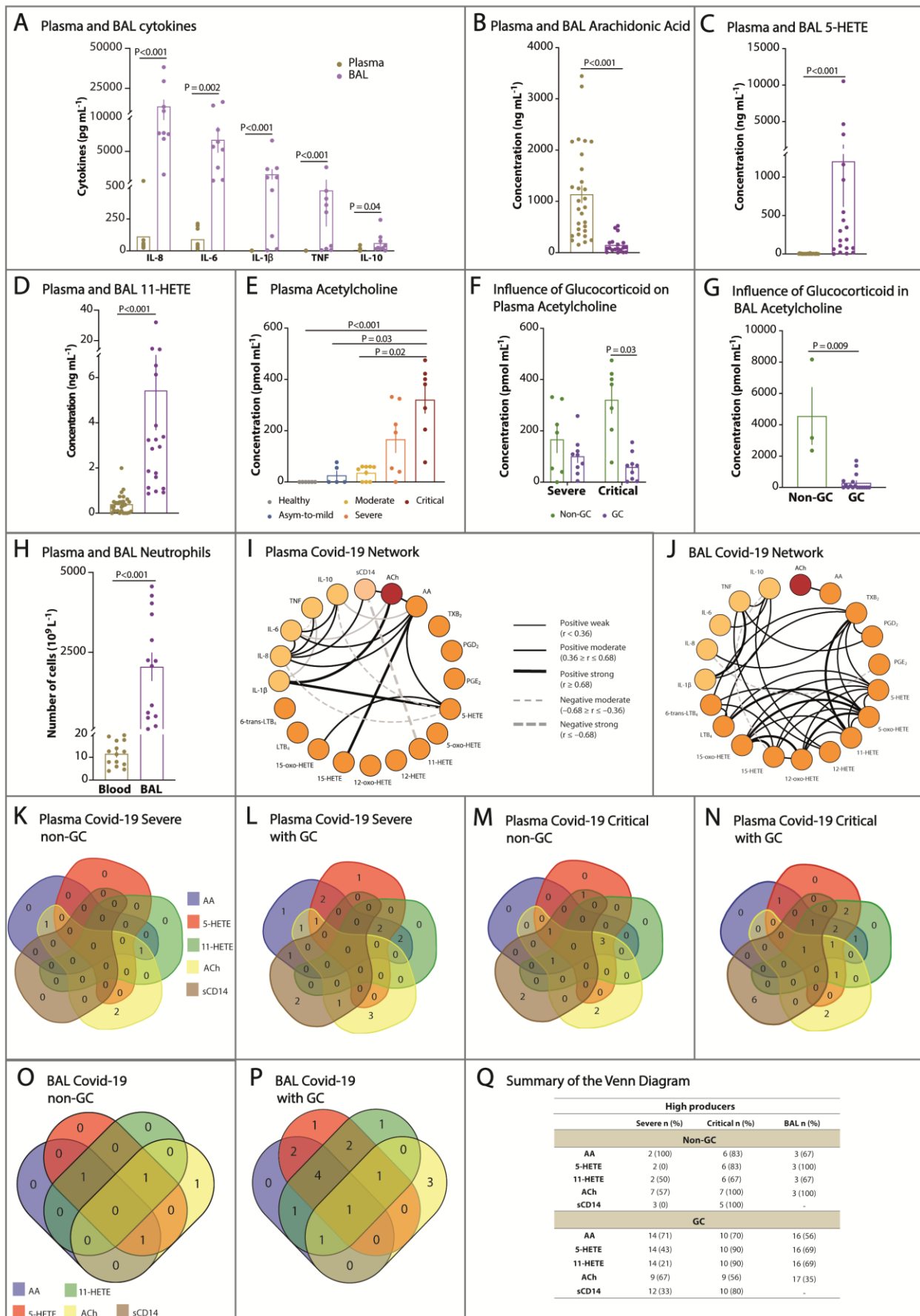
1342

Figure 3



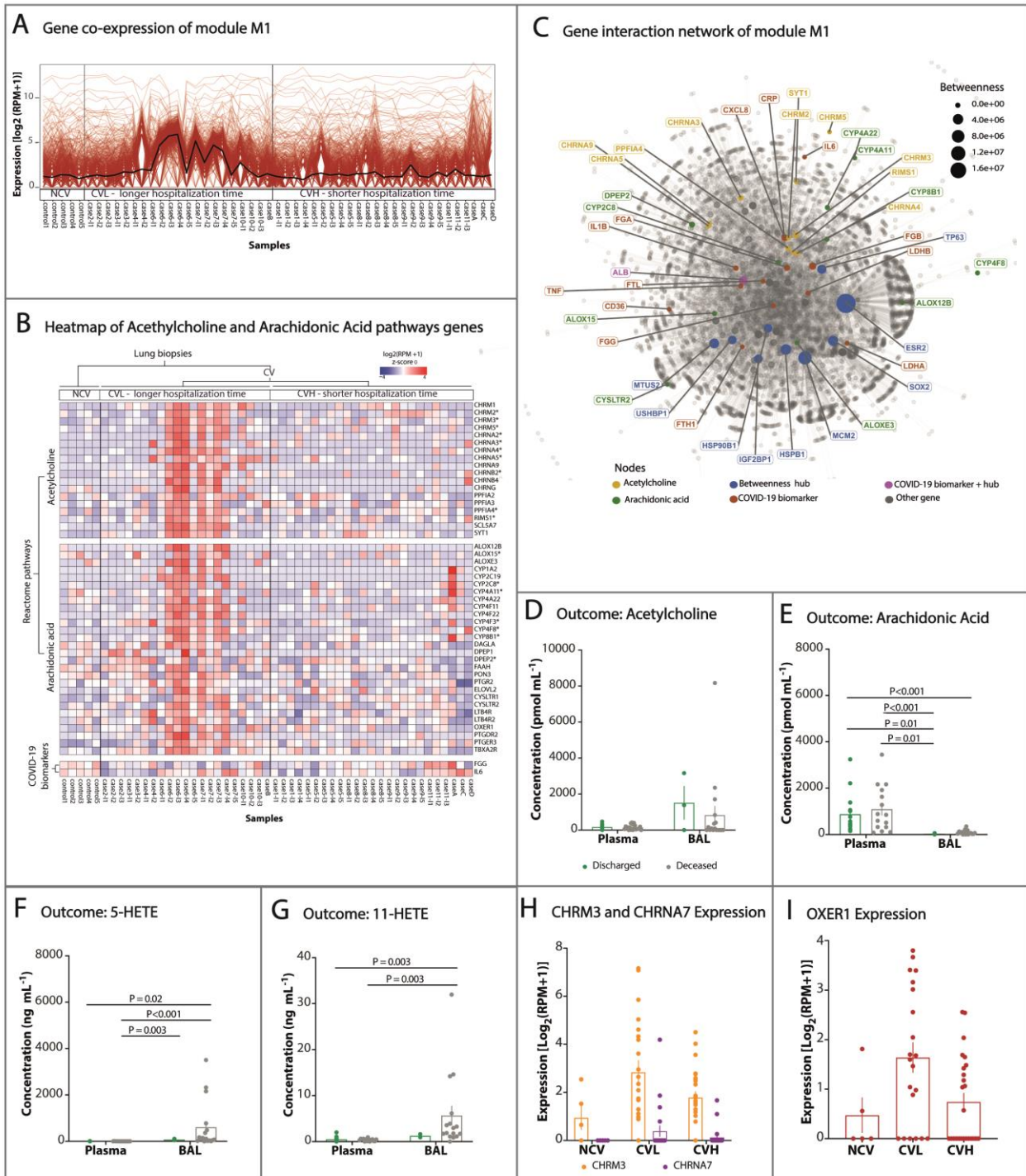
1343

Figure 4



1344

Figure 5



1345 Supplementary Tables

1346 Table S1 – Classification of study participants

Participant's classification	Symptoms, signs, and parameters
<p><i>Group 1</i> Healthy-participants</p>	<ul style="list-style-type: none"> • Negative for SARS-Cov-2 nucleic acid • No clinical signs
<p><i>Group 2</i> Asymp-to-mild</p>	<ul style="list-style-type: none"> • Positive for SARS-Cov-2 nucleic acid and/or serological test • With or without the following symptoms: diarrhea, cough, fever, headache, loss of taste (ageusia)/smell (anosmia), myalgia, nausea, and vomiting
<p><i>Group 3</i> Moderate</p>	<ul style="list-style-type: none"> • Oxygen saturation 94-99 % on room air • Positive for SARS-Cov-2 nucleic acid and/or serological test • Manifestation of mild disease symptoms including dyspnea • Oxygen saturation $\geq 93\%$ on room air • PaO₂/FiO₂ 250-300mmHg • Do not need invasive ventilation: nasal catheter (oxygen 2-4L/min) or oxygen reservoir (oxygen 4-10L/min)
<p><i>Group 4</i> Severe</p>	<ul style="list-style-type: none"> • Positive for SARS-Cov-2 nucleic acid and/or serological test • Admission to intensive-care units • Severe respiratory distress • Oxygen saturation $< 93\%$ on room air • PaO₂/FiO₂ < 250mmHg • Need no-invasive ventilation: oxygen reservoir or non-rebreathing face mask (oxygen 10-15L/min).
<p><i>Group 5</i> Critical</p>	<ul style="list-style-type: none"> • Positive for SARS-Cov-2 nucleic acid and/or serological test • Admission to intensive-care units • Acute respiratory distress syndrome • Need invasive ventilation • PaO₂/FiO₂ < 200mmHg • With or without one or more additional parameters: need hemodialysis, sepsis, septic shock, and multiorgan dysfunction

1347

1348 The participants were classified into five clinical groups (G1–G5): healthy participants (G1) and
 1349 Covid-19 patients (G2 to G5), based on the severity of disease, clinical parameters, patient's
 1350 management, and laboratory findings, following the recommendations from WHO ^{132–137}. These
 1351 classifications were used to define the scale of the clinical progression of patients. The inclusion
 1352 criteria were as follows: (i) signed informed consent form; (ii) fit into one of the five clinical
 1353 groups; (iii) healthy participants must be negative for SARS-CoV-2 nucleic acid; (iv)
 1354 asymptomatic or symptomatic participants must be positive for SARS-CoV-2 nucleic acid and/or
 1355 anti-SARS-CoV-2 antibody; (v) age ≥ 12 years. Participants from groups G1, G2, and G5 were 16

1356 years old or older, while the participants from groups G3 and G4 were 12 years old or older.

1357 Pregnancy was the only exclusion criterion for healthy participants (G1). Abbreviations: FiO_2 ,

1358 fraction of inspired oxygen; PaO_2 , partial pressure of oxygen.

1359

Table S2 – Data of demographic, clinical, and blood findings (n=229)

Baseline Variable	Healthy- participants N= 39	All patients N= 190	COVID-19 care				P value (\$)
			Asym-to-mild N= 43	Moderate N= 44	Severe N= 54	Critical N= 49	
Demographic characteristics							
Age median ± SD, (IQR)	36±16.06 (23-80)	53±18.42 (16-96)	39± 10.74 (20-57)	47± 16.90 (16-92)	62± 15.88 (30-96)	66± 16.63 (20-86)	<0.001
Gender, No. (%)							
Male	19 (49)	107 (56)	18 (42)	25 (57)	30 (56)	34 (69)	0.400
Female	20 (51)	83 (44)	25 (58)	19 (43)	24 (44)	15 (31)	
Comorbidities or coexisting disorders, No. (%)							
Hypertension	5 (13)	77 (41)	5 (12)	11 (25)	40 (74)	21 (43)	<0.001
Dyslipidemia	8 (21)	28 (15)	7 (16)	8 (18)	8 (15)	5 (10)	0.102
Diabetes mellitus	1 (3)	51 (27)	3 (7)	11 (25)	25 (46)	12 (24)	0.002
Obesity	5 (13)	36 (19)	8 (19)	11 (25)	8 (15)	9 (18)	0.450
Neurological Disease	-	20 (11)	-	3 (7)	8 (15)	9 (18)	-
Respiratory Disorders	1 (3)	34 (18)	12 (28)	10 (23)	3 (6)	9 (18)	<0.001
Symptoms, No. (%)							
Dyspnea	-	103 (54)	3 (7)	35 (80)	36 (67)	29 (59)	-
Fever	-	57 (30)	1 (2)	10 (23)	26 (48)	20 (41)	-
Myalgia	-	40 (21)	-	8 (18)	19 (35)	13 (27)	-
Diarrhea	-	48 (25)	13 (30)	13 (30)	13 (24)	9 (18)	-
Cough	-	127 (67)	25 (58)	34 (77)	41 (76)	27 (55)	-
Anosmia	-	59 (31)	27 (63)	19 (43)	7 (13)	6 (12)	-
Dysgeusia	-	57 (30)	25 (58)	19 (43)	8 (15)	5 (10)	-
Headache	-	13 (7)	-	4 (9)	5 (9)	4 (8)	-
Laboratory findings, median ± SD, (IQR)							
Erythrocytes (10 ⁹ L ⁻¹)	4.7±0.48 (4.0-5.8)	4.4±0.88 (1.1-5.9)	4.8±0.46 (3.9-5.9)	4.5±0.71 (2.9-5.9)	4.4±0.99 (1.1-5.9)	3.7±0.67 (2-5.8)	0.0034
Hemoglobin (g dL ⁻¹)	15.0±1.55 (11.3-17.5)	13.1±2.68 (6.5-18.2)	14.5±1.28 (12.0-18.2)	13.9±2.26 (8.4-18.2)	12.9±2.64 (6.8-17.6)	10.7±2.65 (6.5-18.2)	0.001
Leukocytes (10 ⁹ L ⁻¹)	7.5±1.71 (4.1-11.2)	8.8±5.24 (1.6-33.0)	7.3±2.28 (3.2-13.6)	7.7±2.82 (2.6-14.9)	8.6±5.23 (1.6-33.0)	13.2±6.00 (5.2-29.0)	0.042
Neutrophils (10 ⁹ L ⁻¹)	4.2±0.99 (2.4-6.0)	6.3±4.90 (1.6-26.1)	4.1±1.76 (1.8-9.9)	4.9±2.72 (1.8-13.4)	6.8±4.31 (0.24-25.1)	11.4±5.36 (3.7-26.1)	<0.001
Lymphocytes (10 ⁹ L ⁻¹)	2.5±0.85 (1.2-5.1)	1.4±0.93 (0.1-4.3)	2.3±0.67 (1.2-4.3)	2.0±0.90 (0.3-4.2)	1.1±0.82 (0.1-4.1)	0.9±0.54 (0.2-2.6)	<0.001
RNL	1.8±0.56 (1-3.1)	5.1± 14.93 (0.6-115.4)	1.7±0.62 (0.7-3.6)	3±5.61 (0.6-29.7)	6.6±18.23 (1.3-115.4)	11.9±18.30 (3.4-92)	<0.001
Monocytes (10 ⁹ L ⁻¹)	0.5±0.17 (0.3-0.9)	0.5±0.38 (0.0-2.6)	0.5±0.17 (0.3-0.9)	0.4±0.23 (0.1-1.2)	0.5±0.45 (0.0-2.0)	0.5±0.52 (0.0-2.6)	0.207
Platelets (10 ⁹ L ⁻¹)	216±37.34 (129-297)	236± 93.69 (50-635)	227±67.10 (135-474)	234± 88.93 (117-515)	251± 108.5 (85-635)	234±98.67 (50-620)	0.039
Glycemia (mg dL ⁻¹)	90±10.14 (76-113)	113.5±70.37 (28-479)	88±72.88 (65-479)	99.5±39.38 (65-262)	142±78.65 (28-409)	147.5±59.90 (76-301)	<0.001

TTPa (seconds)	26.0±2.49 (21.8-31.7)	26.7±5.65 (0.0-64.1)	26.2±3.28 (20.4-38.6)	26.6±4.80 (18.2-41.4)	27.8±3.66 (20.5-35.2)	26.7±9.38 (0.0-64.1)	0.167
TP (seconds)	13.6±1.68 (12.6-21.7)	13.1±2.1 (0.0-18.1)	13.3±1.29 (12.1-17.5)	13.2±1.17 (11.0-15.2)	12.6±2.65 (0.0-15.7)	13.3±2.81 (0.0-18.1)	0.041
INR	1.12±0.17 (1.0-1.97)	1.1±0.16 (0.0-1.6)	1.1±0.13 (1.0-1.5)	1.1±0.10 (0.9-1.4)	1.1±0.11 (1.0-1.4)	1.2±0.25 (0.0-1.6)	0.106
Hospital support, No. (%)							
Infirmity	-	73 (38)	-	20 (45)	50 (93)	3 (6)	-
Intensive care unit (ICU)	-	53 (28)	-	3 (7)	4 (7)	46 (94)	-
Hospitalization data, No.							
Hospitalization days, median (IQR)	-	10 (1-34)	-	2 (1-23)	9 (1-22)	14 (4-34)	
Infection data, median ± SD, (IQR)							
Infection days	-	5±2.74 (1-16)	-	5±2.54 (1-10)	5±2.97 (2-16)	5±2.58 (1-10)	
Respiratory support received (%)							
Nasal-cannula oxygen	-	58 (31)	-	18 (41)	38 (70)	2 (4)	-
Non-rebreathing mask / Non-invasive ventilation	-	21 (11)	-	-	15 (28)	6 (12)	-
Invasive mechanical ventilation	-	41 (22)	-	-	1 (2)	40 (82)	-
Oxygen saturation median ± SD (IQR)	98.0±2.16 (90-99)	94.0±11.00 (86-100)	98.0±1.79 (93-99)	97.0±4.40 (80-100)	90.5±15.3 (86-99)	91.5±9.84 (66-99)	<0.001
Denouement, No (%)							
Discharge	-	61 (32.1)	-	20 (45.5)	32 (59.3)	9 (18.4)	-
Death	-	65 (34.2)	-	3 (6.8)	22 (40.7)	40 (81.6)	-
Medications No. (%)							
Dexamethasone	-	100 (53)	-	14 (32)	45 (83)	41 (84)	-
Azithromycin	-	98 (52)	1 (2)	18 (41)	52 (96)	28 (57)	-
Ceftriaxone	-	110 (58)	13 (30)	17 (39)	50 (93)	30 (61)	-
Oseltamivir	-	64 (34)	-	4 (9)	37 (69)	23 (47)	-
Cloroquine/Hydroxychloroquine	-	33 (17)	-	3 (7)	13 (24)	17 (35)	-
Anticoagulant	1 (3)	4 (2)	1 (2)	-	-	3 (6)	-
Ivermectin	-	2 (1)	-	1 (2)	1(2)	-	-

Abbreviations: N, number of participants; SD, standard deviation; IQR, interquartile; RNL, ratio between neutrophils and lymphocytes; N (%); TTPa, activated partial thromboplastin time; TP, prothrombin time; INR, international normalised ratio. §Comparison of the control group (healthy participants) with all patients. The values were compared using the χ^2 test and one-way analysis of variance (ANOVA), Mann-Whitney test, and nonparametric t-tests for continuous variables. $p<0.05$ was considered statistically significant.

1367 **Table S3 - Demographic, clinical characteristics and blood findings data from**
 1368 **severe/critical participants of which bronchoalveolar lavage (BAL) were collected**
 1369 **(n=45)**

Baseline Variable BAL	non-Covid-19 Patients N= 13	Covid-19 N= 32	p Value (§)
Demographic characteristics			
Age median ± SD, (IQR)	61±21.2 (20-82)	66.5±17 (25-86)	0,4237
Gender, No. (%)			
Male	4 (30,8)	21 (65,6)	-
Female	9 (69,2)	11 (4,4)	-
Comorbidities or coexisting disorders, No. (%)			
Hypertension	4 (30,77)	16 (51,61)	0,2052
Dyslipidemia	-	2 (6,45)	-
Diabetes <i>mellitus</i>	2 (15,38)	8 (25,81)	0,4517
Obesity	1 (7,69)	3 (9,68)	0,8345
Neurological	2 (15,38)	4 (12,90)	0,8268
Respiratory disorders	7 (53,85)	3 (9,68)	0,0014
Presenting symptoms, No. (%)			
Dyspnea	4 (30,8)	18 (58,1)	-
Fever	-	14 (45,2)	-
Myalgia	-	10 (32,3)	-
Diarrehea	-	7 (22,6)	-
Cough	-	18 (58,1)	-
Hyperactive Delirium	-	-	-
Dysgeusia	-	3 (9,7)	-
Anosmia	-	4 (12,9)	-
Astemia	-	3 (9,7)	-
Laboratory findings, median ± SD, (IQR)			
Erythrocytes (10 ¹² L ⁻¹)	2.7±0.94 (1,6-5,2)	3.5±0.70 (2-5,3)	0,0175
Hemoglobin (g dL ⁻¹)	8.7±2.93 (4,6-15,2)	10.3±2.19 (6,5-16,2)	0,0319
Leukocytes (10 ⁹ L ⁻¹)	11.5±15.44 (7,8-62,4)	11.8±6.70 (4,6-29,0)	0,7848
Neutrophils (10 ⁹ L ⁻¹)	8.6±11.18 (4,5-45,5)	9.6±5.95 (3,3-26,1)	0,9842
Lymphocytes (10 ⁹ L ⁻¹)	1.2±1.08 (0,3-4,4)	0.9±0.54 (0,4-2,2)	0,2127
RNL	7±21.15 (2,6-73)	11.0±10.05 (3,36-43,5)	0,2925
Monocytes (10 ⁹ L ⁻¹)	0.6±0.51 (0,3-1,8)	0.6±0.55 (0-2,6)	0,5627
Platelets (10 ⁹ L ⁻¹)	254±165.8 (71-553)	252±86.8 (50-414)	0,4519
Glycemia (mg dL ⁻¹)	151.5±85.91 (9,8-376)	148±58.23 (76-300)	0,5848
TP	13.2±1.97 (11,5-17,1)	13.1±3.34 (0-18,1)	0,8464
TTPa	25.5±6.30 (22,6-46)	25.2±10.96 (0-64,1)	0,6380
INR	1.1±0.18 (0,1-1,5)	1.2±0.30 (0-1,6)	0,9632
Respiratory support received (%)			
Oxygen Saturation median ± SD (IQR)	94±6.41 (78-100)	91±10.36 (66-99)	0,0500
Hospitalization data, No.			
Hospitalization days, median (IQR)	22±11.41 (6-43)	14±15.36 (5-34)	0,0888
Infeccions data, median ± SD, (IQR)			
Infection days	4±3,27 (2-10)	6±2,46 (0-11)	0,3166
Denouement, No (%)			
Discharge	9 (69,2)	4 (12,9)	-
Death	4 (30,8)	28 (87,5)	-
Medications No. (%)			
Dexamethasone	2 (15,38)	26 (83,87)	<0,0001
Azithromycin	1 (7,69)	2 (6,45)	0,8816
Ceftriaxone	10 (76,92)	25 (78,13)	0,9300
Oseltamivir	1 (7,69)	16 (51,61)	0,0063
Cloroquine/Hydroxycloquine	1 (7,69)	10 (32,26)	0,0860
Anticoagulant	-	-	-
Ivermectin	-	-	-

1370

1371 Abbreviations: N, number or values; SD, standard deviation; IQR, minimum and maximum
1372 values; RNL, ratio between neutrophils and lymphocytes; N (%); TTPa, activated partial
1373 thromboplastin time; TP, prothrombin time; INR, international normalised ratio. §Comparison of
1374 the Covid-19 negative patients group with Covid-19 positive patients. The values were compared
1375 using the χ^2 test and one-way analysis of variance (ANOVA), Mann-Whitney test, and
1376 nonparametric t-tests for continuous variables. $p < 0.05$ was considered statistically significant.
1377

1378 **Table S4 – List of genes related to acetylcholine and arachidonic acid**
1379 **pathways and Covid-19 biomarkers founded in co-expression module M1**

Gene (symbol)	Gene (name)	Pathway or Biomarker
CHRM2	cholinergic receptor muscarinic 2	
CHRM3	cholinergic receptor muscarinic 3	
CHRM5	cholinergic receptor muscarinic 5	
CHRNA2	cholinergic receptor nicotinic alpha 2 subunit	
CHRNA3	cholinergic receptor nicotinic alpha 3 subunit	
CHRNA4	cholinergic receptor nicotinic alpha 4 subunit	Acetylcholine
CHRNA5	cholinergic receptor nicotinic alpha 5 subunit	
CHRNB2	cholinergic receptor nicotinic beta 2 subunit	
PPFIA4	PTPRF interacting protein alpha 4	
RIMS1	regulating synaptic membrane exocytosis 1	
ALOX15	arachidonate 15-lipoxygenase	
CYP4F3	cytochrome P450 family 4 subfamily F member 3	
CYP4A11	cytochrome P450 family 4 subfamily A member 11	
CYP8B1	cytochrome P450 family 4 subfamily B member 1	
CYP4F8	cytochrome P450 family 4 subfamily F member 8	Arachidonic acid
CYP2C8	cytochrome P450 family 2 subfamily C member 8	
CYP1A1	cytochrome P450 family 1 subfamily A member 1	
DPEP2	dipeptidase 2	
ALB	Albumin	
CRP	C-reactive protein	
CXCL8 (IL8)	C-X-C motif chemokine ligand 8	Biomarker (COVID-19)
FGA	fibrinogen alpha chain	
FGB	fibrinogen beta chain	
IL1 β	interleukin 1 beta	

1380
1381 Co-expression analysis generated five different co-expression gene modules (M1 to
1382 M5) and only in M1 we identified genes that encoding proteins associated to
1383 cholinergic receptors (muscarinic and nicotinic), ACh release cycle, and AA
1384 metabolism. In addition, the M1 module also contains some biomarkers related to

1385 Covid-19 severity (albumin, C-reactive protein, IL-8, fibrinogen, and IL1 β)

1386 21,34,138,139.

1387 **Table S5 - Treatment of severe and critical Covid-19 patients with glucocorticoids**
 1388 **does not alter the levels of plasmatic cytokines and circulating neutrophils and**
 1389 **lymphocytes**

	Severe non-GC N=3	Severe GC N=39	<i>P value</i> (#)	Critical non-GC N=4	Critical GC N=17	<i>P value</i> (§)
Parameters, median \pm SEM, (IQR)						
IL-8	31.7 \pm 12.6 (13.6-56.0)	26.3 \pm 4.97 (2.8-186.4)	0.454	26.86 \pm 6.5 (10.2-41.8)	113.2 \pm 48.8 (13.1-661.9)	0.144
IL-6	42.7 \pm 20.1 (4.80-73.2)	54.9 \pm 14.19 (3.3-414.1)	0.782	46.4 \pm 13.2 (24.7-81.7)	317.7 \pm 160.3 (11.3-2510)	0.410
IL-1	2.5 \pm 2.5 (0.0-7.6)	0.1 \pm 0.05 (0.0-1.7)	0.104	0.9 \pm 0.9 (0.0-3.6)	0.5 \pm 0.3 (0.0-3.8)	0.874
TNF	0.0 \pm 0.0 (0.0-0.0)	0.01 \pm 0.1 (0.0-0.3)	>0.999	0.8 \pm 0.8 (0.0-3.1)	0.04 \pm 0.04 (0.0-0.7)	0.191
IL-10	1.0 \pm 0.5 (0.4-2.1)	2.7 \pm 0.4 (0.3-9.1)	0.165	2.3 \pm 1.1 (0.8-4.3)	7.5 \pm 2.6 (0.1-45.1)	0.229
Neutrophils	56.5 \pm 20.8 (15.0-77.5)	80.5 \pm 1.7 (38.6-97.0)	0.097	79.9 \pm 3.8 (73.1-89.0)	85.6 \pm 1.5 (70.1-93.0)	0.197
Lymphocytes	9.7 \pm 1.6 (8.0-13.0)	12.0 \pm 0.9 (2.0-27.8)	0.490	10.9 \pm 2.2 (5.0-14.7)	7.9 \pm 1.0 (4.0-20.5)	0.156
RNL	5.7 \pm 2.2 (1.9-9.4)	10.2 \pm 1.6 (2.2-47.5)	0.403	9.0 \pm 2.7 (5.1-16.6)	13.3 \pm 1.5 (3.4-23.3)	0.140

1390

1391 Abbreviations: N, number of participants; SEM, standard error of the mean; IQR, interquartile;
 1392 RNL, ratio between neutrophils and lymphocytes. §Comparison of the severe non-GC group with
 1393 the severe GC group, and the critical non-GC group with the critical GC group. The values were
 1394 compared using the χ^2 test, one-way analysis of variance (ANOVA), Mann-Whitney test, and
 1395 nonparametric t-tests for continuous variables. $p < 0.05$ was considered statistically significant.

1396 As shown in the table, glucocorticoid therapy in severe Covid-19 patients did not show a
 1397 statistically significant influence on the plasma levels of the cytokines evaluated in our study. The
 1398 use of glucocorticoids and their impact on the production of inflammatory molecules is closely
 1399 associated with several factors, such as the dose, duration, and time of initiation of therapy, since,

1400 in the critical stages of Covid-19, no beneficial effects of glucocorticoids have been observed in
1401 the inflammation control and patient outcome ^{70,71}.

1402 **Table S6 - Impact of glucocorticoid therapy in the outcome of hospitalized Covid-**
1403 **19 patients**

No, (%)	Moderate N=23		Severe N=54		Critical N=49	
	Discharge N=20	Death N=3	Discharge N=32	Death N=22	Discharge N=9	Death N=40
non-GC	7 (35)	0 (0)	4 (12.5)	3 (13.6)	4 (44.4)	9 (22.5)
GC	13 (62)	3 (100)	28 (87.5)	19 (86.4)	5 (55.6)	31 (77.5)

1404

1405 Abbreviations: N, number of participants (%).

1406 Hospitalised Covid-19 patients from the moderate, severe, and critical groups were
1407 administered glucocorticoid (GC) therapy or not (non-GC) (methylprednisolone; range 40 to 500
1408 mg/kg/day, or dexamethasone; range 1.5 to 6.0 mg/kg/day, by intravenous route). Most
1409 hospitalised patients were treated with glucocorticoids (moderate [69.6%], severe [87.0%], and
1410 critical [73.5%]). All moderate non-GC-patients were discharged, while GC patients had a
1411 mortality rate of 18.8%. In addition, the mortality rates for severe-GC (40.4%) and critical-GC
1412 (86.1%) patients were higher than those for moderate-CG patients. The discharge rates of non-
1413 GC patients vary according to the clinical categorization (100.0%, 57.1%, and 30.8% for
1414 moderate, severe, and critical, respectively). Hospitalised Covid-19 patients from our cohort
1415 showed fewer benefits of glucocorticoid therapy than those reported in the RECOVERY trial ⁶⁸,
1416 but similar benefits to those described in the CoDEX trial conducted in Brazil ⁶⁹. This reduction
1417 of glucocorticoid benefits could be associated with several factors, including a low mean
1418 PaO₂:FiO₂ ratio and an overload of the health systems of countries with limited resources, such
1419 as Brazil ⁶⁹, as well as glucocorticoid dose, initiation, and duration of therapy ^{70,71}.

1420

1421 **Table S7 – Analysis of the potential interference of Covid-19-confounding variables**
 1422 **on the correlation between high plasma levels of cholinergic and lipid mediators and**
 1423 **Covid-19 severity.**

Confounding variables	Healthy participants	Asym-to-mild	Moderate	Severe	Critical	P value (\$)
Lipid mediators (AA, 5-HETE, and 11-HETE)						
No	17	10	11	16	11	
Age, mean (IQR)	33 (27-44)	33 (26-43)	39 (30-48)	57 (48-78)	71 (57-78)	<0.001
Gender, No (%) Male						0.795
Female	7 (41.2)	5 (50.0)	6 (54.5)	7 (43.8)	7 (63.6)	
Diabetes, No (%)	10 (58.8)	5 (50.0)	5 (45.5)	9 (56.2)	4 (36.4)	
Hypertension, No (%)	1 (5.9)	1 (10.0)	3 (27.3)	6 (37.5)	2 (18.2)	0.183
Obesity, No (%)	2 (11.8)	0 (0.0)	0 (0.0)	12 (75.0)	6 (54.5)	<0.001
	4 (23.5)	2 (20.0)	3 (27.3)	2 (12.5)	1 (9.1)	0.7788
ACh						
No	6	5	4	6	8	
Age, mean (IQR)	30 (24-56)	42 (38-46)	48 (39-57)	75 (63-79)	65 (52-74)	0.026
Gender, No (%) Male						0.290
Female	4 (66.7)	3 (60.0)	2 (50.0)	1 (16.7)	6 (75.0)	
Diabetes, No. (%)	2 (33.3)	2 (40.0)	2 (50.0)	5 (83.3)	2 (25.0)	
Hypertension, No. (%)	0 (0.0)	1 (20.0)	1 (25.0)	3 (50.0)	1 (12.5)	0.282
Obesity, No. (%)	2 (33.3)	2 (40.0)	1 (25.0)	5 (83.3)	3 (37.5)	0.360
	1 (16.7)	1 (20.0)	0 (0.0)	0 (0.0)	2 (25.0)	0.767

1424
 1425 We analysed some confounding variables associated with Covid-19, such as comorbidities (Diabetes
 1426 mellitus, hypertension, and obesity) and risk factors (advance age and gender)^{51,140}, using data from
 1427 participants whose plasma levels of lipid mediators (AA, 5-HETE, and 11-HETE) and ACh were measured.
 1428 Lipid mediators data came from Covid-19 patients and healthy participants presented in Figure 1 (Panels:
 1429 F, G, and H), while ACh data came from glucocorticoid-non-treated Covid-19 patients presented in Figure
 1430 4E. Age and hypertension or only age are potential confounding variables on the correlation between high
 1431 plasma levels of lipid mediators or ACh and Covid-19 severity, because (i) age had significant Spearman's
 1432 correlation with AA ($r=0.36$; $P=0.0042$), 5-HETE ($r=0.36$; $P=0.0042$), and ACh ($r=0.37$; $P=0.0485$); and
 1433 (ii) hypertensive patients had significantly increased plasma levels of AA ($p=0.0062$ - Mann-Whitney test).
 1434 §Kruskal-Wallis or Fisher's tests were used to compare the differences between all clinical categories. Data
 1435 are expressed as median (IQR - interquartile range) or number (% - percentages), and $P < 0.05$ was
 1436 considered statistically significant.

1437 **Table S8 - Analysis of the potential interference of Covid-19-confounding**
 1438 **variables on the correlation between high ACh levels in severe/critical**
 1439 **patients, treated or not with glucocorticoids, and Covid-19 severity.**

Confounding variables	Severe (Plasm)			Critical (Plasm)			Critical (BAL)		
	non-GC	GC	P value (\$)	non-GC	GC	P value (\$)	non-GC	GC	P value (\$)
No	6	10		8	8		3	17	
Age, median (IQR)	75 (63-79)	68 (55-76)	0.415	65 (52-74)	76 (60-79)	0.316	74 (72-80)	62 (53-76)	0.243
Gender, No (%) Male	1 (16.7)	7 (70.0)	0.118	6 (75.0)	6 (75.0)	1.000	2 (66.7)	11 (64.7)	0.920
Female Diabetes, No (%)	5 (83.3)	3 (30.0)	1.000	2 (25.0)	2 (25.0)	0.569	1 (33.3)	6 (35.3)	0.450
Hypertension, No (%)	4 (40.0)	6 (60.0)	1.000	1 (12.5)	3 (37.5)	0.619	3 (100.0)	3 (17.6)	0.073
Obesity, No (%)	2 (20.0)	8 (80.0)	1.000	3 (37.5)	5 (62.5)	1.000	0 (0.0)	3 (17.6)	1.000

1440

1441 Here we used the same confounding variables associated with Covid-19 described on Table
 1442 S7. This analysis was based on plasma and BAL cholinergic mediator (ACh) data from
 1443 severe/critical Covid-19 patients, treated (GC) or not (non-GC) with glucocorticoids, and
 1444 reported in Figure 4 (Panels: F and G). None of the confounding variables tested had significant
 1445 potential to interfere with the glucocorticoid-therapy ability to reduce the high plasma and BAL
 1446 ACh levels in severe/critical patients. §Mann-Whitney or Fisher’s tests were used to compare
 1447 the differences between severe and critical clinical categories. Data are expressed as median
 1448 (IQR - interquartile range) or number (% - percentages), and $P < 0.05$ was considered
 1449 statistically significant.

1450 **Table S9 - Impact of Covid-19 confounding variables on the comparative analysis**
 1451 **between high levels of lipid mediators in plasma and BAL samples from severe and**
 1452 **critical patients.**

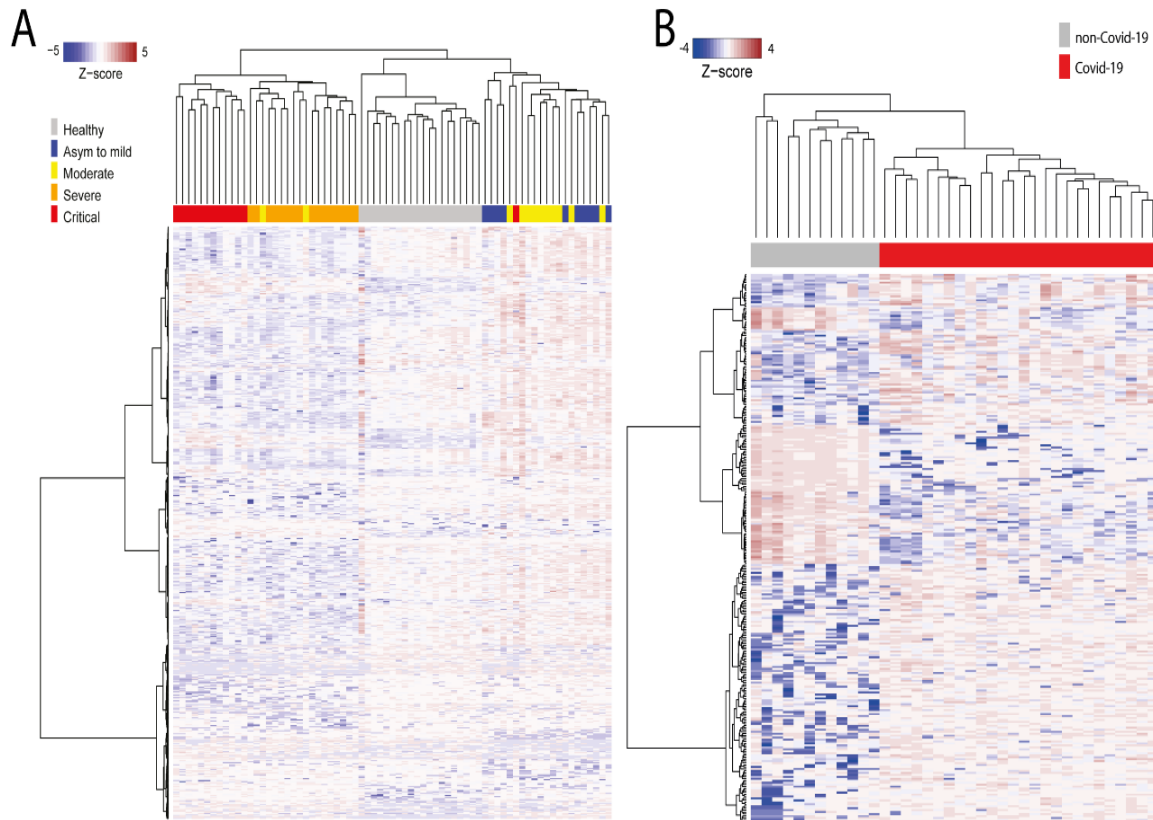
Confounding variables	Severe/Critical (Plasm)	Severe/Critical (BAL)	P value (\$)
No	25	18	
Age, median (IQR)	60 (53-77)	64 (52-83)	0.6395
Gender, No. (%) Male			0.1394
Female	14 (56.0)	14 (77.8)	
Diabetes, No. (%)	11 (44.0)	4 (22.2)	
Hypertension, No. (%)	7 (28.0)	5 (27.8)	0.9872
Obesity, No. (%)	16 (64.0)	9 (50.0)	0.3586
	3 (12.0)	4 (22.2)	0.4274

1453

1454 We used the same confounding variables associated with Covid-19 reported on Table S7. This
 1455 analysis was based on plasma and BAL levels of lipid mediators (AA, 5-HETE, and 11-HETE)
 1456 from severe/critical Covid-19 patients reported in Figure 4 (Panels: B, C, and D). None of the
 1457 confounding variables tested had significant potential to interfere with the comparison between
 1458 altered plasm and BAL levels of lipid mediators in severe/critical patients. §Mann-Whitney, chi-
 1459 square, or Fisher’s tests were used to compare the differences between severe and critical patients.
 1460 Data are expressed as median (IQR - interquartile range) or number (% - percentages), and P <
 1461 0.05 was considered statistically significant.

1462 **Supplementary Figures**

1463 **Figure S1 – Metabolic signatures of plasma and BAL samples from patients**
1464 **infected or not with SARS-CoV-2.**



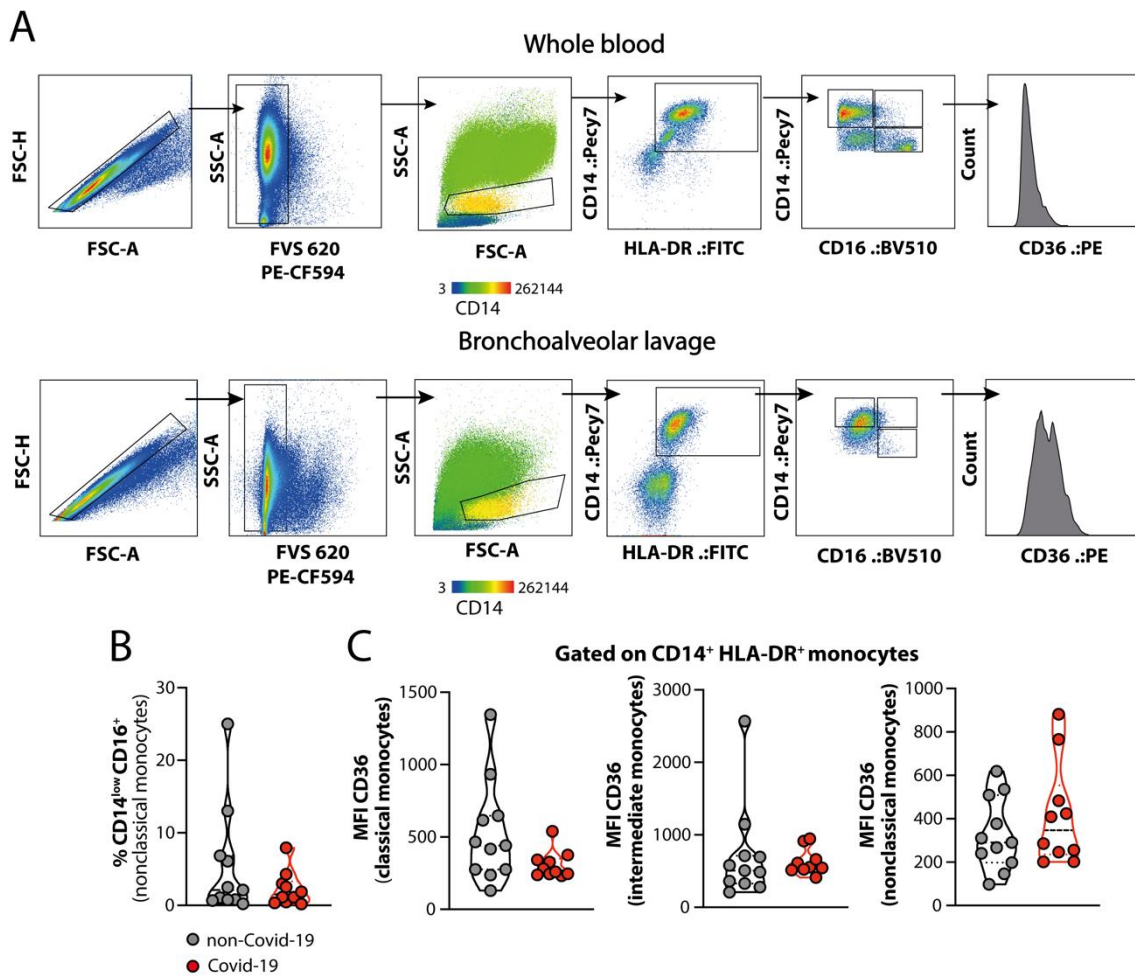
1465

1466 Hierarchical clustering based on different characteristics of abundant metabolites
1467 (ANOVA-FDR <0.1) between controls and patients positive for SARS-CoV-2 at different stages
1468 of the disease in plasma (A) and non-Covid-19 versus Covid-19 BAL patients (B). In (A), the
1469 clinical classification of Covid-19 was: healthy participants (n=20), asymptomatic-to-mild
1470 (n=10), moderate (n=12), severe (n=16), and critical (n=13) groups. In (B), the same analysis was
1471 performed with data from BAL samples of non-Covid-19 (n=12) and Covid-19 (n=26) patients.
1472 The detection levels of metabolites were defined using Z-score normalisation.

1473 The analysis of hierarchical clustering (A) shows highly different metabolomic profiles
1474 in the plasma for each group of individuals according to disease severity. BAL analysis (B) of
1475 samples from Covid-19 patients demonstrated an increase in the abundance of metabolites
1476 compared to non-Covid-19 individuals. The results indicated that SARS-CoV-2 infection induces

1477 changes in the metabolic profile of humans. Our data are in agreement with previous results
1478 showing virus-induced metabolic reprogramming in the host. The increased abundance of
1479 metabolites and their pathways, such as free fatty acids and amino acids, was correlated to the
1480 increase in viral proliferation, since these biomolecules can act as building blocks and fuel for
1481 this process¹⁴¹⁻¹⁴³.

1482 **Figure S2 - Gating strategy used for flow cytometry analysis of monocyte subsets**
1483 **and CD14/CD36 expression**



1484

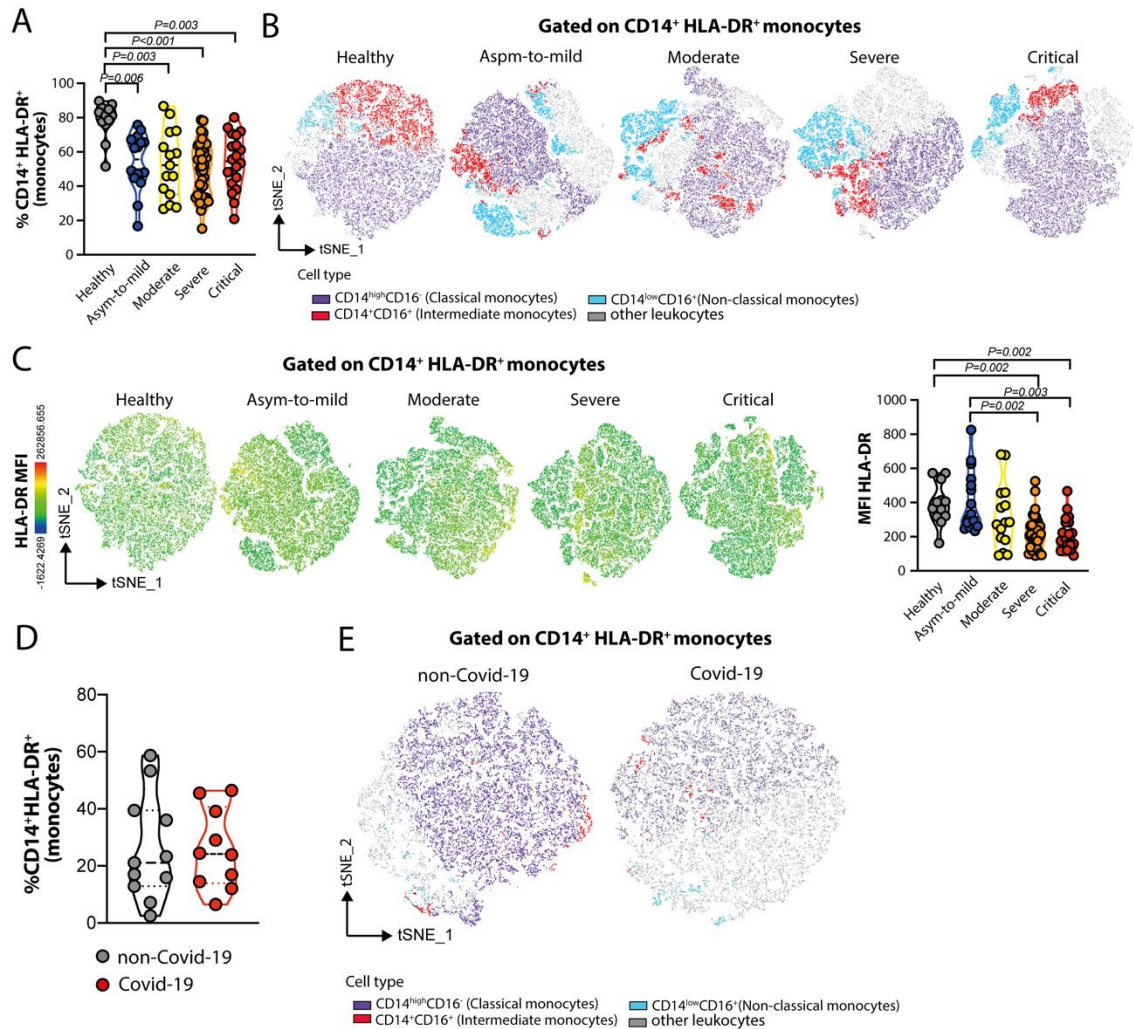
1485

1486 In (A), dot plots show a representative gating strategy for the analysis of FSC-H/FSC-A,
1487 SSC-A/FVS-620 (viable cells), and SSC-A/FSC-A, followed by CD14⁺HLA-DR⁺ monocytes and
1488 the classical (CD14^{high}CD16⁻), intermediate (CD14⁺CD16⁺) or non-classical CD14^{low}CD16⁺
1489 subsets, with subsequent CD36 mean fluorescence intensity (MFI) in whole blood (upper panel)
1490 and bronchoalveolar lavage fluid (BAL, bottom panel). In (B), a violin plot shows the frequency
1491 of non-classical monocytes from BAL of non-Covid-19 and Covid-19 patients. In (C), CD36 MFI
1492 in classical, intermediate, and non-classical monocytes from BAL of non-Covid-19 and Covid-
1493 19 samples. Differences between groups were calculated using the Mann-Whitney test.

1494 The membrane markers and gating strategies used to define the different monocyte
1495 subpopulations in the blood and BAL samples were adapted from a previous publication (ref). In
1496 BAL, there was a tendency to reduce non-classical monocytes in Covid-19 patients compared to
1497 non-Covid-19 patients (Figure 2SB), as well as a decrease in CD36 expression in classical and
1498 intermediate monocytes (Figure 2SC), although the difference was not statistically significant.
1499 Although not significantly, this reduction may have a biological importance. These data are
1500 similar to the profile observed in the blood monocytes of Covid-19 patients (Figure 3J).

1501 **Figure S3 - Determination of monocyte subsets in the blood and BAL samples from**
 1502 **non-Covid-19 and Covid-19 patients**

1503



1504

1505

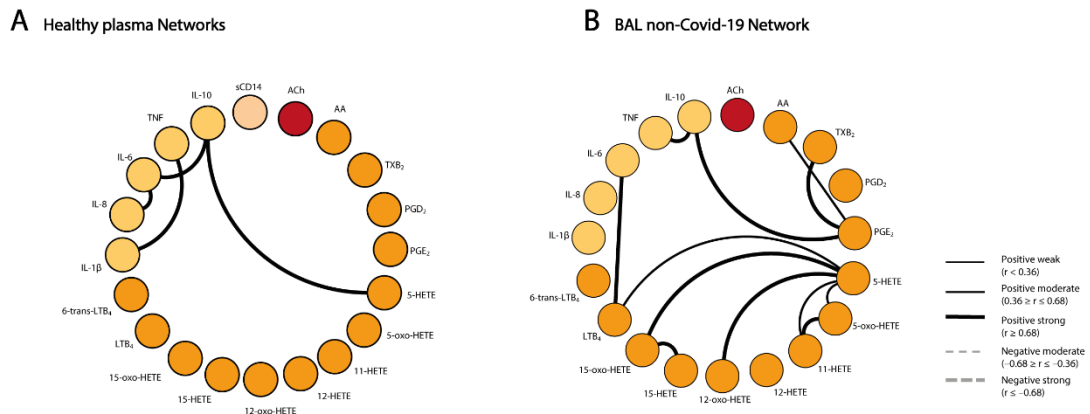
1506

1507 Peripheral blood from healthy participants (n=12), and asymptomatic-to-mild
 1508 (n=15), moderate (n=15), severe (n=35), or critical (n=20) patients, and BAL from Covid-
 1509 19 (n=10) and non-Covid-19 (n=11) participants were collected and used for the
 1510 characterisation of monocyte subpopulations by flow cytometry and t-distributed
 1511 stochastic neighbour embedding (t-SNE) analysis. (A) Frequency of CD14⁺HLA-DR⁺
 1512 cells. (B) t-SNE evaluation of classical (CD14^{high}CD16⁻), intermediate (CD14⁺CD16⁺),

1513 and non-classical CD14^{low}CD16⁺ blood monocytes in Covid-19 patients, categorised
1514 according to disease severity. (C) Colour mapping t-SNE and violin plot showing the
1515 mean fluorescence intensity (MFI) of HLA-DR expression in the circulating monocytes
1516 of Covid-19 subjects. In (D) and (E), samples of BAL from non-Covid-19 and Covid-19
1517 patients were evaluated to determine the frequency of CD14⁺HLA-DR⁺ cells and
1518 classical, intermediate, or non-classical monocyte subsets, respectively. Differences
1519 among groups were calculated using the Kruskal-Wallis test with Dunn's multiple
1520 comparison post-test, and the corresponding values are indicated in the figures.

1521 In comparison to healthy participants (Figure S3A, S3B, and 3SC), a significant
1522 reduction was observed in the intermediate monocyte population, as well as in the
1523 expression of HLA-DR molecules in the blood of Covid-19 patients, depending on
1524 disease severity. The diminishment of HLA-DR in monocytes correlated with TNF values
1525 obtained in the blood of patients positive for SARS-CoV-2 (Figure 2P; principal article),
1526 since monocytes with a pro-inflammatory profile are the main producers of this cytokine
1527 ¹⁴⁴. Similarly, reduced intermediate monocytes were found in the BAL of patients positive
1528 for Covid-19 (Figure S3E). Interestingly, these patients also had a significant increase in
1529 the production of IL-8, IL-10, and IL-6 cytokines in the blood and BAL, as shown before
1530 (Figure 2M, 2N, and 2Q and Figure 4A; principal article). The high production of
1531 cytokines, especially IL-6, in patients with Covid-19, has been correlated with a decrease
1532 in the expression of HLA-DR in monocytes, while the therapeutic inhibition of IL-6 re-
1533 established the expression of this molecule in those individuals¹⁴⁵

1534 **Figure S4 - Biomarker networks in non-Covid-19 and healthy participants**



1535

1536 A network of interactions between lipid mediators, ACh, sCD14, and cytokines in (A)

1537 healthy participants (n=39) and (B) BAL non-Covid-19 participants (n=13). Network layouts of

1538 personalised biomarkers were set up to identify the relevant association in healthy and non-Covid-

1539 19 participants. Each connecting line denotes a significant correlation between a pair of markers.

1540 Continuous lines represent positive correlations, while dashed lines represent negative

1541 correlations ($p < 0.05$). The degree of significance is represented by the thickness of the line.

1542 Correlations were determined using Spearman's test; the values of r and p were used to classify

1543 the connections as weak ($r \leq 0.35$, $p < 0.05$), moderate ($r = 0.36-0.67$, $p < 0.01$), or strong ($r \geq 0.68$,

1544 $p < 0.001$). The absence of a line indicates the non-existence of the relationship. To evaluate the

1545 relationship between levels of lipid mediators, ACh, sCD14, and cytokines in non-Covid-19, a

1546 series of correlation analyses were performed.

1547 When comparing the interactions analysed between the molecules of the healthy and non-

1548 Covid-19 groups, we observed that (A) In the blood of healthy individuals, the interactions were

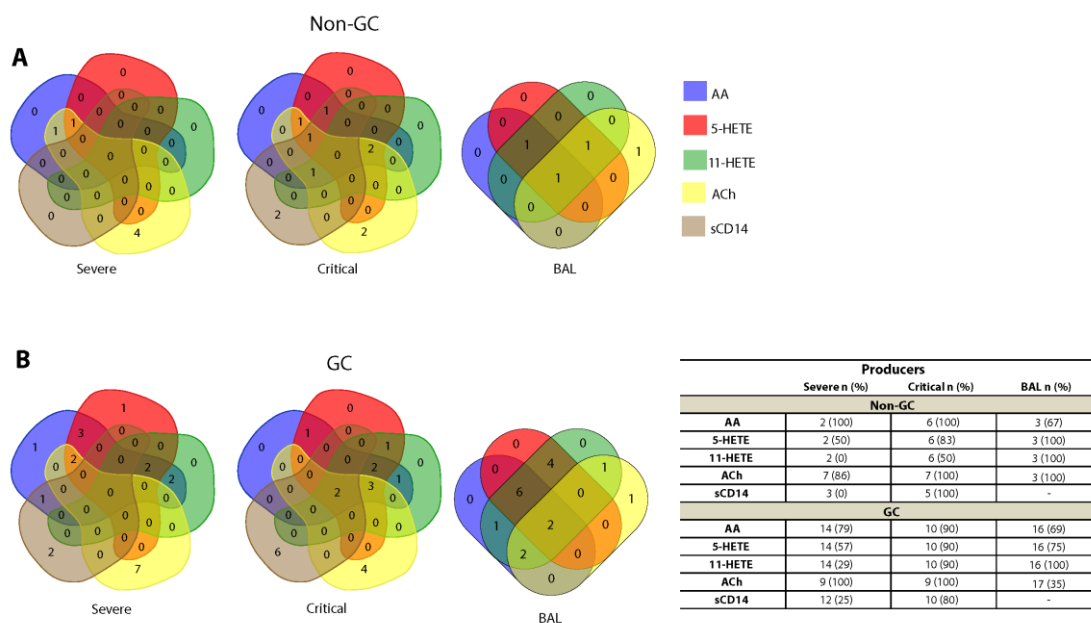
1549 found to occur mainly between cytokines (IL-1 β , TNF, IL-8, IL-6, and IL-10) and the lipid

1550 mediator 5-HETE. (B) In the BAL samples from hospitalised non-Covid-19 patients, lipid

1551 mediators were found to mediate these interactions and influence the clinical outcomes of this

1552 group of patients.

1553 **Figure S5 – Treatment of severe and critical SARS-CoV-2-infected patients with**
1554 **glucocorticoids inhibits ACh release**



1555

1556

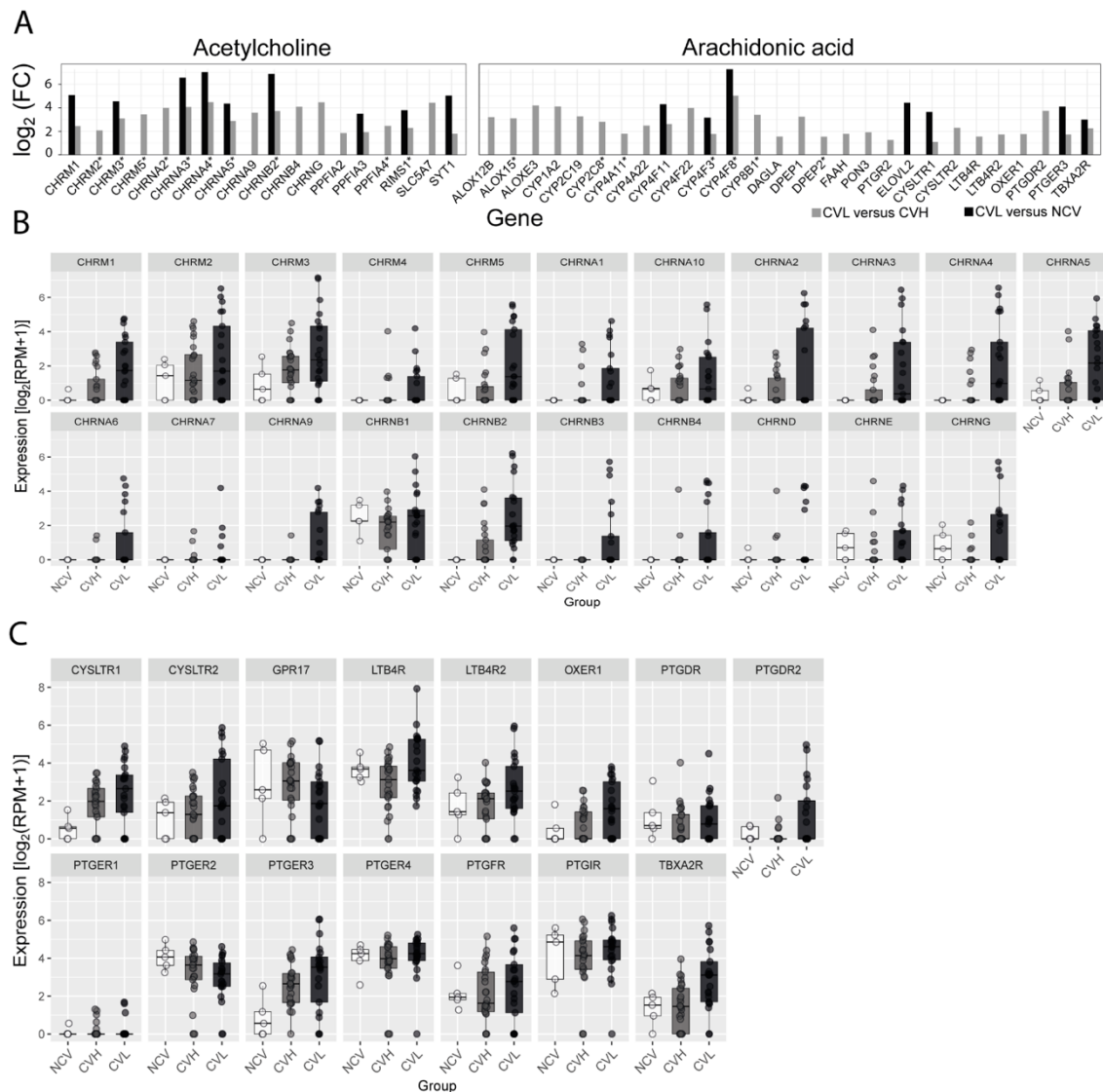
1557 The production of lipid mediators and the shedding of sCD14 in patients with Covid-19
1558 at the severe and critical stages was not modified by treatment with glucocorticoids (GC).
1559 However, a marked reduction was observed in ACh release. Intersection analysis depicted in
1560 Venn diagrams revealed the number of patients producing AA, 5-HETE, 11-HETE, ACh, or
1561 sCD14, above the control (healthy participants) values, in the absence (A) or presence (B) of GC
1562 therapy. The table shows the number (*n*) of plasma or BAL samples from Covid-19 patients at
1563 the severe and critical stages of disease, for each mediator. The percentages shown in parentheses
1564 represent the frequency of patients producing the respective mediator for the corresponding
1565 sample number.

1566 The Venn diagrams show the intersections of AA, 5-HETE, 11-HETE, ACh, and sCD14s
1567 in Covid-19 patients at the severe and critical stages of the disease, in both blood and BAL. No
1568 significant changes were observed in the quantification of lipid mediators or sCD14, comparing
1569 patients treated with or without glucocorticoids (Figure S5A and FigureS5B). Interestingly,
1570 critically ill patients treated with glucocorticoids showed a 20% and 65% reduction in the ACh

1571 concentration in both blood and BAL samples, respectively, compared to patients who were not
1572 administered drugs (Figure S5B). While a decrease in free-AA and its metabolites (5-HETE and
1573 11-HETE) has not been reported in the literature, some studies have demonstrated the beneficial
1574 effects of the use of glucocorticoids in other respiratory syndromes, having been found to reduce
1575 the production of AA-derived mediators^{72,146}. In agreement with our results, there is no evidence
1576 to support corticoid treatment for Covid-19¹⁴⁷. Data related to the effect of glucocorticoids on
1577 ACh release in viral infections are scarce. However, according to our previous findings on
1578 scorpion envenomation³, glucocorticoid treatment should be initiated early after infection to block
1579 the release of lipid mediators, which could lead to the inhibition of premature ACh release. On
1580 the contrary, the late administration of GC could place patients at a point of no return, with early
1581 ACh release impacting vital organs, damaged by the negative impacts of this neurotransmitter
1582 before GC administration. Moreover, it should be considered that, in Covid-19, other unknown
1583 mechanisms may control ACh release, in addition to the COX-2 dependent metabolites.

1584 **Figure S6 - Differential expression and profile of genes involved in AA and ACh**
1585 **pathways from SARS-CoV-2 deceased patients**

1586



1587

1588

1589 Abbreviations: CVL, Covid-19 low viral load; CVH, Covid-19 high viral load; NCV,
1590 non-Covid-19 viral load^{9,50,110,113}.

1591 As shown in (A), DEGs were upregulated in CVL versus CVH patients and CVL
1592 versus NCV patients. The transcript expression of cholinergic receptors (muscarinic and
1593 nicotinic) (B) and eicosanoid receptors (C) was normalised in the NCV, CVH, and CVL
1594 groups. CVL patients displayed increased pulmonary levels of expression of genes

1595 associated with the ACh and AA pathways, encoding for cholinergic receptors, the ACh
1596 release cycle, AA metabolism, and eicosanoid receptors, compared to CVH or NCV
1597 patients. The expression profile of some genes may favour inflammatory events, such as
1598 upregulated cholinergic and eicosanoid receptors (CHRM3, CHRNA3, CHRNA5, and
1599 OXER1) and low levels of the anti-inflammatory cholinergic receptor (CHRNA7)
1600 ^{9,50,110,113}.